Transportation Research Part D 154 (2026) 105291

Contents lists available at ScienceDirect

Transportation Research Part D

journal homepage: www.elsevier.com/locate/trd

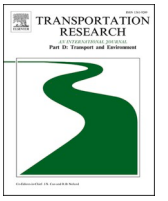

A Risk-Based simulation approach to assessing seaport resilience against cyclone hazards

Massoud Mohsendokht [a], Ali Mokhtari-Moghadam [a], Huanhuan Li [a,b], Christos Kontovas [a], Chia-Hsun Chang [a], Zhuohua Qu [c], Zaili Yang [a,*]

[a] Liverpool Logistics, Offshore and Marine (LOOM) Research Institute, Liverpool John Moores University, Liverpool, UK
[b] School of Engineering, University of Southampton, Southampton, UK
[c] Liverpool Business School, Liverpool John Moores University, Liverpool, UK

ARTICLE INFO

Keywords:
Cyclone
Risk-based simulation
Vulnerability
Seaport
Climate change
Economic loss

ABSTRACT

Seaports face intensifying cyclone risks due to climate change, yet comprehensive risk-based approaches quantifying the probability and consequences of such impacts on port functionality and economic performance remain scarce. This study integrates probabilistic modelling of cyclone occurrence with asset-level fragility and downtime analysis to estimate functional degradation while quantifying direct physical damage and associated economic impacts on port operations. The Port of Kaohsiung, in southwestern Taiwan, serves as the case study, drawing on terminal records and historical cyclone data to simulate throughput loss under varying cyclone types and intensities. The research findings enable port authorities to assess port capacity to withstand and recover from disruptions and to design targeted adaptation and restoration strategies. By combining realistic data, advanced simulation, and a holistic resilience perspective, this study makes significant contributions to the development of a cost-effective decision-support tool for long-term port sustainability.

1. Introduction

Due to their coastal locations, seaports are highly vulnerable to a wide variety of natural catastrophes. These hazards range from seismic events and cyclones to rising sea levels, flooding, and storm surges, all of which can disrupt seaport activities in unpredictable ways. When a seaport is affected by one of these catastrophes, its superstructures, systems, sub-systems, equipment, and relevant components, such as berths, quay walls, quay cranes, trucks, yard cranes, and electrical substations can suffer significant physical damage. This damage not only leads to immediate operational delays but often results in long-term financial losses due to extensive repair and recovery efforts. In some extreme cases, a seaport may never return to its full capacity, even after years of recovery, leading to long-lasting disruptions to regional and global supply chains (Yamamura, 2016).

Given the increasing frequency and intensity of natural hazards, largely driven by climate change, assessing the vulnerability of ports to these events has become an urgent task, as recent empirical evidence shows that cyclones and associated storm surge and extreme rainfall already cause considerable operational disruptions across dozens of ports worldwide, and authoritative climate assessments project further increases in tropical cyclone rainfall intensity, the likelihood of compound coastal flooding, and storm surge impacts as sea level rises, implying that cyclone related port downtime risks will become more frequent and severe in the coming

* Corresponding author at: James Parsons Building, Byrom Street, Liverpool, L3 3AF, UK.
E-mail address: z.yang@ljmu.ac.uk (Z. Yang).

https://doi.org/10.1016/j.trd.2026.105291
Received 15 October 2025; Received in revised form 6 January 2026; Accepted 17 February 2026
Available online 2 March 2026

decades (Calvin et al., 2023; Yang et al., 2025; Xia et al., 2024; Asariotis et al., 2024). However, this process is complex and challenging for several reasons, as follows:

1) Uncertainty in predicting hazards and impacts: accurately predicting natural hazards such as storms, flooding, or earthquakes, as well as their potential impacts on seaport infrastructure, remains a major challenge. The unpredictability of such events, combined with the long-term nature of climate change, makes it difficult to anticipate the full extent of their consequences.
2) Confidentiality of port operations: port operators often face concerns regarding the confidentiality of their operational data. The competitive nature of the maritime industry means that sensitive information about port capacities, vulnerabilities, and risk mitigation strategies is often not publicly disclosed. This lack of transparency complicates efforts to assess resilience across different ports and share best practices.
3) Scarcity of historical data: another significant challenge is the limited availability of historical data on past hazards that have affected ports. Much of this information is not publicly available due to privacy concerns, security issues, or proprietary data restrictions. This data scarcity makes it difficult to build comprehensive models of seaport vulnerability and resilience.

Despite these challenges, recent research efforts have advanced the use of simulation-based techniques to deal with this issue (Cao and Lam, 2018; Na and Shinozuka, 2009; Zhang et al., 2025). Simulation models are particularly useful for predicting the impacts of natural hazards and estimating both direct and indirect losses due to disruptions. By simulating seaport operations under different hazard scenarios, these models can help identify vulnerabilities and design more resilient systems.

However, the use of simulation-based techniques to cover the full scope of port vulnerability and resilience, from operational degradation to direct and indirect economic losses, remains underdeveloped. Many studies either focus narrowly on how hazards affect operational performance while omitting loss modelling, or rely heavily on subjective inputs due to sparse hazard/impact data and provide limited validation against post-event evidence (Dragović et al., 2017; Mohsendokht et al., 2025).

To extend the current body of knowledge, this study aims to develop a hybrid, simulation-based framework to assess seaport resilience in terms of both operational functionality and economic vulnerability by quantifying not only the direct and indirect physical damage from cyclone hazards but also the resulting economic losses. The new framework integrates (i) probabilistic hazard modelling to estimate the frequency-intensity distributions of different cyclone types, (ii) vulnerability analysis of port superstructures via asset-specific fragility curves, and (iii) operations modelling to derive throughput loss and translate it into direct and indirect economic impacts. Within this scope, the definition of seaport resilience adopted in this paper aligns with the prevailing viewpoint in the maritime community, namely the capacity of a port to withstand disturbances, maintain its essential structure and operations, adapt to evolving conditions, and restore service to a satisfactory level within acceptable time and financial constraints following a disruption (Mohsendokht et al., 2025). In this study, resilience is operationalised implicitly through its core contributing capacities. The absorptive capacity is captured through the robustness assessment of critical equipment under extreme wind loading, quantified via fragility curves and damage states. The adaptive capacity is reflected in operational responses, including vessel rerouting, continued use of undamaged cranes, and reconfiguration of remaining critical-path components. The restorative capacity is characterised by the duration and progression of post-event recovery, represented through restoration curves for critical port assets. Taken together, these elements allow resilience to be examined across the full disruption timeline, from hazard onset through to full functional recovery.

The new framework and its supporting models are demonstrated and validated using the Port of Kaohsiung (i.e., Terminal 7) in southwestern Taiwan, a cyclone-prone hub as a case study, with a risk-informed vulnerability assessment tailored to its assets and operations. The framework enables port authorities and stakeholders to characterise risk, evaluate capacity to withstand and recover from disruptions, and design cost-effective adaptation and recovery strategies. By combining realistic data, advanced simulation techniques, and a holistic view of resilience, it offers a practical decision-support tool for strengthening the long-term sustainability and reliability of seaports under increasing climate-related hazards.

The remainder of the paper is organized as follows: Section 2 reviews the literature on hazard analysis and vulnerability assessment. Section 3 details the proposed methodology and overall framework. Section 4 describes the case study and required data. Section 5 reports the results, discusses the findings and their implications. Finally, Section 6 concludes and outlines directions for future research.

2. Literature review

2.1. Hazard identification in seaports facing climate change

Seaports, by virtue of their coastal siting and direct exposure to open waters, are subject to a wide range of natural hazards that can disrupt their normal operations. Typical hazards include tropical cyclones, storm surge, coastal flooding, riverine flooding, high winds and extreme waves/swell, tsunamis, fog/low visibility, extreme temperatures, seismic events, landslides, and volcanic ashfall. Given this breadth, hazard types are categorised and ranked by risk parameters such as frequency of occurrence and potential consequences (e.g., expected throughput loss, asset damage, downtime, and safety implications), for screening-level risk prioritisation and subsequent fragility and restoration modelling (Wang et al., 2020; Yang et al., 2018).

Table 1 compiles recorded natural hazards affecting seaports, supported by global evidence on occurrence rates and severity. To aid interpretation, selected historical case studies are included with estimated operational impacts, such as berth closures, crane outages, navigational restrictions, and yard inundation. This approach facilitates the linking of hazard characteristics to observable performance degradation.

Table 1
Global overview of natural hazards disrupting seaport operations.

Hazard type	Description	Typical Frequency (Global)	Downtime	Real case	Representative sources
Pluvial flooding	Intense rainfall causing surface water to inundate port areas, disrupting operations and damaging the infrastructures.	Several events per year in wet climates; return period typically 1–5 years for disruptive rainfall	Less than 3 days	UK (2013–14) floods damaged port assets USD 2 m (Port of Hull)	(Prieto et al., 2024; UNDRR, 2019; Verschuur et al. 2023)
Fluvial flooding	River overflows, inundating port facilities, halting cargo movement and causing structural and navigational hazards.	Decadal-scale events (5–20 year return period) depending on basin	days-weeks	Mississippi (2011), more than USD 0.3 bn to Gulf ports.	(Becker et al., 2013; Merz et al., 2010)
Cyclones	Hurricanes or typhoons combining high winds, storm surge, and waves, severely damaging port infrastructure and operations.	10–20 cyclones per year globally, regionally seasonal	days-weeks	Hurricane Ike (2008), USD 2.4 bn to Texas ports; Typhoon Maemi (2003), toppled 6 quay cranes, disrupted several container berths for weeks, total loss of USD 100–200 million.	(Verschuur et al., 2023; Pan, 2015)
Sea rise	Elevated sea levels from storms overtopping defences, flooding docks, quays, and storage areas.	Typically, once every 10–50 years for major surges (exposure higher in NW Europe, East Asia)	hours-days	UK east-coast surge (1953), King's Lynn (1953) (more than USD 1 bn)	(Verschuur et al., 2023; Pugh and Woodworth, 2014)
Extreme maritime conditions	Non-storm high waves, winds, or extreme temperatures forcing temporary port closures due to safety risks.	Several days per year at exposed ports	hours-days; cause > 40% of short closures	Port Elizabeth, SA: recurrent wave-height shutting the port for 12–24 h on nearly 40% of days per year.	(Izaguirre et al., 2021; PIANC, 2020)
Earthquakes & liquefaction	Seismic shaking and soil failure collapsing quay walls and piers, causing prolonged port downtime.	Low frequency, but concentrated in seismic belts; multi-decadal (hot-spots Chile, Japan, Med.)	Weeks-months (infrastructure rebuild)	Kobe (1995), USD 3–4 bn port damage.	(Na and Shinozuka, 2009; Iai, 2019)
Tsunamis	Sudden, powerful sea waves inundating ports, destroying equipment, docks, and infrastructure with catastrophic impact.	Rare; major events once per several decades globally	Weeks-months	Tōhoku (2011): USD 12 bn port damage; ~ USD 3.4 bn trade loss per day	(Chua et al., 2024)
Volcanic ash / eruptions	Ash falls and pyroclastic debris contaminating waterways, clogging machinery, and halting port operations.	Localized, less than 1% of ports near active centers	Hours-weeks (ash clean-up)	Tonga (2022) ash closed Nukuʻalofa port forcing a 72-hour shutdown.	(Miller et al., 2016)

Among major natural hazards affecting ports worldwide, tropical cyclones constitute the leading risk for approximately one quarter of ports and can rapidly cripple regional trade corridors. Recent multi-hazard modelling indicates that cyclones account for the largest single share of expected annual asset losses in the port sector, their outsized role in port disruption (Izaguirre et al., 2021; Verschuur et al., 2023; Xu et al., 2024).

Other hazards must also be taken seriously; however, they typically involve shorter durations, lower frequencies at most sites, or more localised footprints. As a result, their operational consequences are often more constrained in time and space than those associated with basin-scale cyclone systems. Pluvial and fluvial flooding is widespread, exposing the majority of ports; however, typical operational downtime is measured in hours to a few days and can often be mitigated through drainage improvements and elevation of critical assets (Christodoulou et al., 2020). Sea-level-rise-driven coastal flooding is a dominant long-term threat at many sites, but it tends to manifest gradually (Bayazit, 2025). Extreme maritime conditions (e.g., high waves and swell) frequently trigger short-duration safety closures, usually lasting hours to a day rather than weeks. Earthquakes and tsunamis can be catastrophic, with prolonged rebuild times, but their occurrence is geographically concentrated and far less frequent for most ports.

As a result, tropical cyclones warrant elevated priority in seaport risk management because they combine multiple stressors, such as extreme winds, storm surge, and large waves that can simultaneously damage quay cranes, storage yards, and access channels, resulting in multi-day to multi-week outages and costly sediment clean-ups. This combination of substantial economic losses and extended operational downtime makes cyclones one of the most dangerous threats to seaports in vulnerable regions (Verschuur et al., 2023).

2.2. Seaport vulnerability assessment against natural hazards

Seaport performance under disruption is commonly framed in terms of reliability, vulnerability, functionality loss, robustness, survivability, safety, and security. These constructs address overlapping technical aspects of operational functionality but differ in emphasis. Reliability concerns sustained service delivery; vulnerability denotes susceptibility to loss; functionality loss indicates the reduction in the delivered service level relative to its pre-disruption baseline; robustness reflects performance under stress; survivability focuses on maintaining a minimally acceptable level of function; safety addresses harm prevention; and security pertains to intentional threats (Mohsendokht et al., 2025).

Current approaches to seaport loss estimation and vulnerability assessment usually revolve around probabilistic techniques (Mohsendokht et al., 2026; Wan et al., 2024;), physics-based modelling (Tian et al., 2024), and simulation approaches (Zhang et al., 2025). Within probabilistic frameworks, Bayesian networks (BNs) are widely employed to represent causal dependencies and propagate uncertainty. For example, the resilience of the Port of Catoosa to multiple disruptions has been analysed by decomposing resilience into absorptive, adaptive, and restorative capacities, mapping each capacity to corresponding strategies, and quantifying their aggregate effect on port functionality (Hosseini and Barker, 2016). Comparable BN applications across diverse case studies, together with other probabilistic methods, further underscore this approach's suitability for uncertainty quantification in seaport vulnerability evaluation (Camus et al., 2019; Wang et al., 2023; Hossain et al., 2019).

Physics-based approaches employ mechanistic models that solve the governing equations for both the hazard process (e.g., tsunami, storm surge, long-period waves) and the port response (e.g., harbour agitation, moored-ship motions, quay-wall and soil-structure interaction). Typical outputs include time series and spatial fields of water levels, currents, wave spectra, resonance amplitudes, vessel motions, and structural demands. These results are then mapped to functional consequences, such as downtime and damage states (Borrero et al., 2015; Jorge Rosa-Santos and Taveira-Pinto, 2013; Rego and Li, 2010; Sun and Niu, 2021; Romano-Moreno et al., 2023). As an example, in a relevant study, numerical simulations of tsunami scenarios in the South China Sea are used to estimate inundation depths, runup, and basin oscillations, thereby identifying ports at risk. Port-specific risk is quantified by the direct economic losses associated with trade interruption over the disruption period (Chua et al., 2024).

In simulation-based approaches, hazard mechanics and port operations are emulated to estimate downtime, throughput loss, and associated economic impacts. Studies typically employ system dynamics (Zhang et al., 2025), discrete-event simulation (Folkman et al., 2021), and agent-based modelling (Li et al., 2024). Na and Shinozuka (2009) developed a framework that integrates a container-terminal operations model with component fragility functions to propagate earthquake-induced damage into service disruption. A similar approach has been applied to typhoon impacts at Shenzhen Port, linking wind and sea-state scenarios to equipment outages, queuing delays, and both direct and indirect economic losses (Cao and Lam, 2018). Recently, the use of digital twins has also gained traction. In a study, a BIM-integrated (building information modelling), synthetic-data–calibrated digital twin was developed for simulation-based seaport vulnerability assessment, enabling resilience and sustainability analysis for bulk terminals, demonstrated on biomass operations at the Port of Tyne (Zhu et al., 2025).

2.3. Research gaps

Based on the literature review presented in previous sections, existing studies on seaport loss estimation and vulnerability assessment generally fall into three main categories: probabilistic approaches, physics-based modelling, and simulation-based methods.

Probabilistic risk studies typically estimate failure probabilities at aggregated system or asset levels and focus on exceedance metrics. However, they often provide limited linkage to scenario-specific operational consequences or monetised loss estimates. Physics-based approaches explicitly model hazard generation and loading mechanisms (e.g., wind, storm surge, and waves) together with the physical response of port assets. While these methods offer high physical fidelity, they are usually data- and computationally

intensive, asset-specific, and difficult to generalise or scale across multiple scenarios and complex port systems. Simulation-based approaches, on the other hand, provide valuable insights into system performance and operational dynamics, but many existing implementations rely on deterministic assumptions or expert-elicited inputs for damage, downtime, and recovery processes. As a result, hazard uncertainty is often underrepresented, and the linkage between operational degradation and economic loss remains weak. These limitations are particularly evident in cyclone-induced port loss assessments, where sparse empirical damage and downtime data further increase reliance on subjective assumptions.

In addition to the limited number of studies in this field, the above methodological gaps motivated the present research. Accordingly, this study proposes a novel hybrid probabilistic-deterministic methodology that explicitly integrates equipment degradation probabilities induced by cyclones with simulation-based modelling of their consequences on port throughput. This study models cyclone hazards probabilistically across frequency and intensity, develops asset-specific fragility and downtime distributions to furnish defensible, data-driven inputs for terminal-operations modelling, and quantifies both functional degradation (throughput shortfalls) and economic consequences (direct damage and indirect downtime costs). The framework prioritises physical realism where it materially affects outcomes, propagates uncertainty from hazards through vulnerability and recovery to performance, and delivers decision-ready indicators, such as confidence-bounded downtime and cost estimates. The proposed approach supports resilience planning and the evaluation of adaptation options under current and future climate conditions.

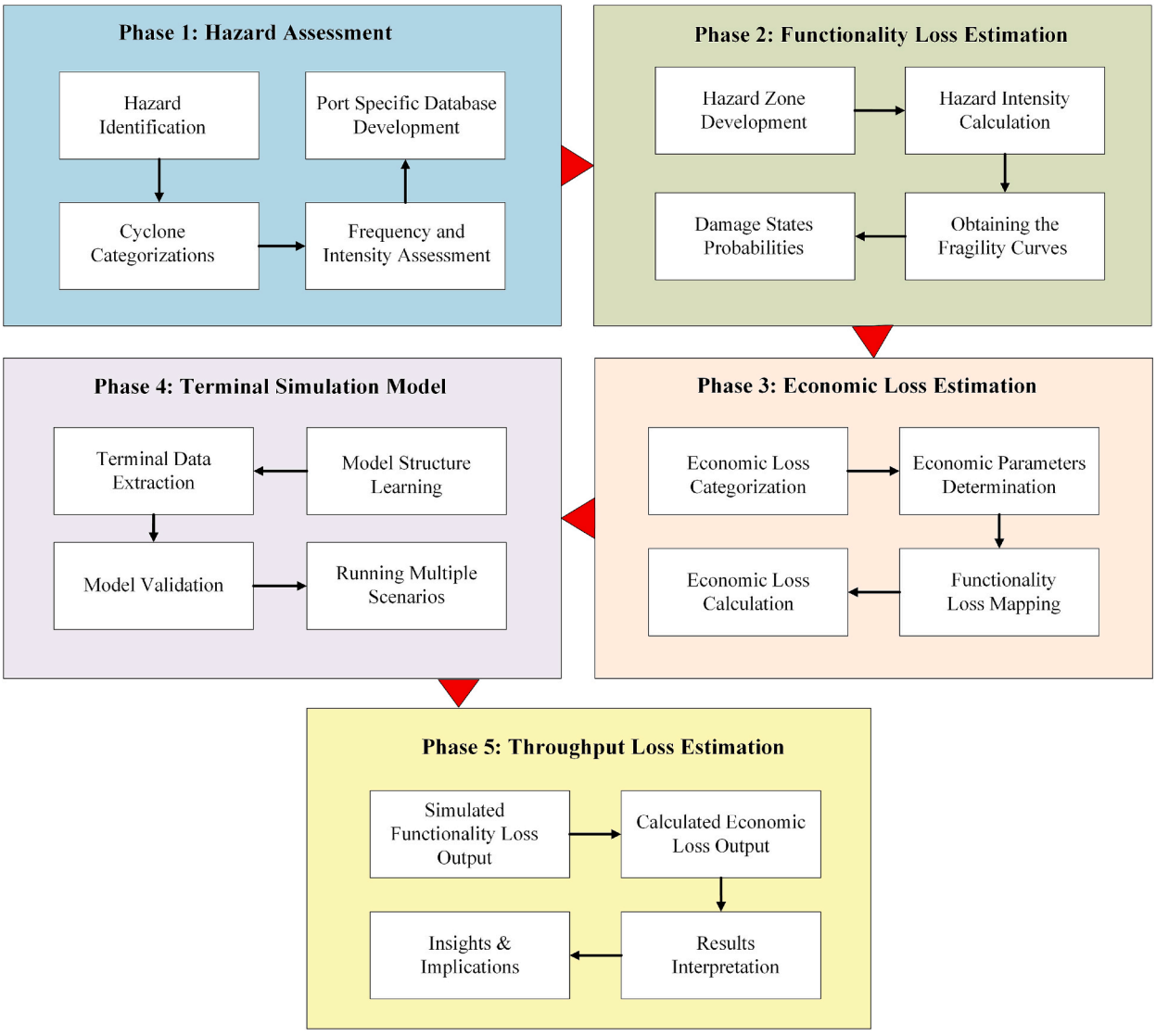

Fig. 1. The overall framework of the proposed methodology.

3. Methodology

This section presents a novel integrated risk-based simulation framework for vulnerability assessment of seaports facing cyclone hazards, which accounts for various dimensions of functionality and economic losses. Fig. 1 illustrates the overall framework of the proposed methodology, structured into five consecutive phases. The subsequent sections elaborate on the detailed procedures of the phases.

3.1. Hazard assessment

As discussed earlier, cyclones are among the most dangerous natural hazards for seaports in vulnerable regions, causing substantial economic losses and prolonged operational downtime. A cyclone is a broad, generic term referring to a rotating low-pressure atmospheric system characterized by inward-spiralling winds around a central pressure minimum. Cyclones are commonly classified into three main categories based on their formation mechanisms, thermal structure, and latitudinal location, namely tropical, subtropical, and extratropical cyclones.

Tropical cyclones develop primarily over warm ocean waters in low latitudes, typically between about 5° and 30° north or south of the equator and derive their energy predominantly from latent heat release associated with deep convection (Holton and Hakim, 2013). These systems exhibit a warm-core structure and are referred to regionally as hurricanes, typhoons, or tropical cyclones, depending on the basin of occurrence. When referring to a specific type of cyclone, the terminology must reflect its regional classification and meteorological context. In this study, tropical cyclone is adopted as the preferred and generic scientific term to describe the hazard. Regionally, tropical cyclones with the wind speed higher than 33 m/sec are referred to as typhoons in the Northwest Pacific and hurricanes in the Atlantic and Eastern Pacific basins. Therefore, this study focuses on characterizing the different types of tropical cyclones and evaluating their potential impacts on port infrastructure and operations.

To this end, the Japan Meteorological Agency (JMA) intensity classification was adopted, which is based on 10-minute sustained

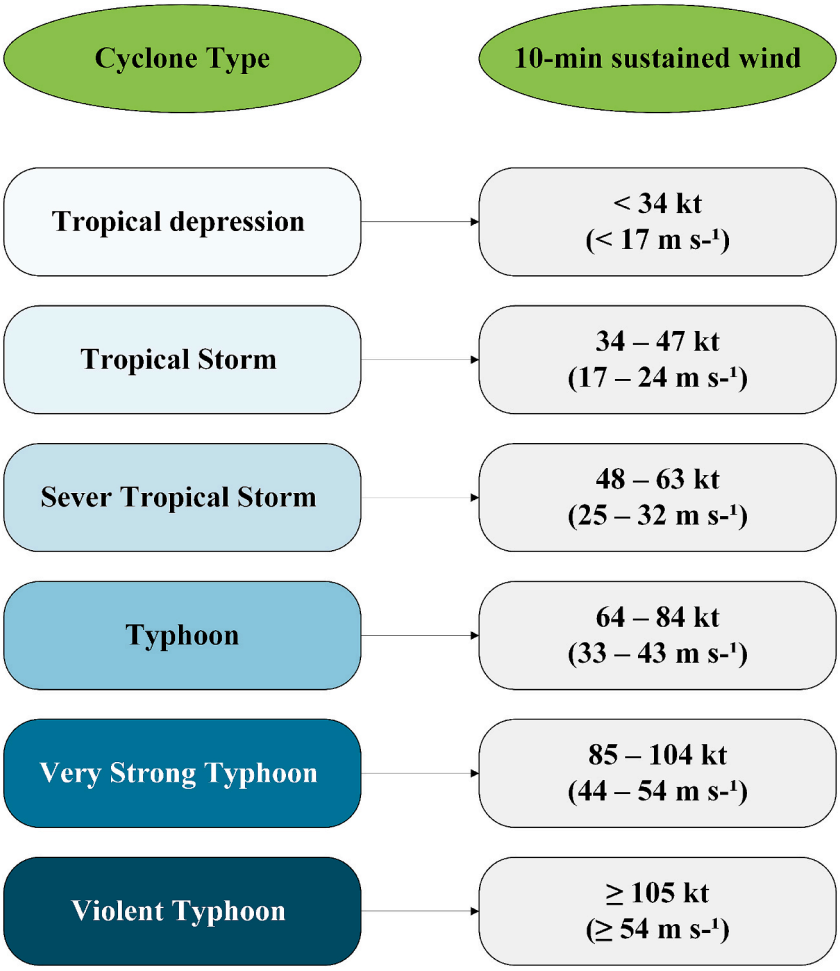

Fig. 2. Cyclone categories based on JMA classification.

wind speeds in accordance with World Meteorological Organization (WMO) practice (Japan Meteorological Agency, 2023). This approach ensures consistency with Western North Pacific records and local warning standards while offering finer analytical resolution (Song et al., 2010). The classification thresholds also align with the WMO Typhoon Committee's wind-bracket definitions, as documented in the CWA RDC28 Typhoon Database web tool (TDB, 2024). The resulting six-tier classification comprises: Tropical Depression (TD), Tropical Storm (TS), Severe Tropical Storm (STS), Typhoon (TY), Very Strong Typhoon (VST), and Violent Typhoon (VTY). Fig. 2 presents these categories along with their defining characteristics.

Categorizing the impacts of cyclones by geospatial zones is required for a realistic hazard assessment. Each zone is associated with a characteristic hazard profile, which ranges from the eyewall's maximum winds and storm surge to gale-force wind fields and rainband effects, and finally to peripheral swell and residual surge. Each hazard type can trigger distinct failure modes in port infrastructure and operations (Schott et al., 2019; Emanuel, 2006; 2005; Jian et al., 2019; Huang et al., 2024).

To this end, cyclone impact zones were stratified into two principal distance classes, direct strike (0–200 km) and vicinity strike (>200–400 km), to reflect distinct hazard regimes observed in previous studies (Lu et al., 2022; Zong and Chen, 1999; Cao and Lam, 2018). The direct strike region encompasses the most intense meteorological features, including the eyewall, radius of maximum wind (RMW $<$ 50 km), secondary eyewalls, inner rainbands, and the principal gale field. These features exhibit steep radial gradients in wind speed and precipitation, which are typically concentrated within 200 km of the cyclone centre. This distance is consistent with the operational warning systems, and hazard classification schemes that define significant impact zones within 125–232 km of the storm track (Chavas and Emanuel, 2010). Accordingly, the 0–200 km range was divided into four 50 km intervals to enhance the spatial resolution and capture rapid gradients and transitions across the storm core and inner wind field, as follows: Ring 1: 0–50 km, Ring 2: 50–100 km, Ring 3: 100–150 km, and Ring 4: 150–200 km.

Beyond 200 km, cyclone hazards become increasingly dependent on storm size rather than inner-core dynamics. This vicinity strike zone is characterized by flatter radial gradients and greater influence from the outer wind field. Hazards in this region, particularly storm surge, scale with storm size and expand more gradually with distance. Therefore, the region beyond 200 km was divided into broader 100 km intervals, as Ring 5 (200–300 km) and Ring 6 (300–400 km), to capture variability in storm size while avoiding unnecessary segmentation where gradients diminish. The outer cutoff at 400 km was selected based on evidence from satellite-based climatology, indicating that the majority of structural variability and hazard significance is contained within this range, while gradients beyond 400 km are weak and largely negligible (Knaff et al., 2007).

Having categorized cyclones by intensity and distance, the next step is to determine the frequency of each cyclone type within the defined ring zones. This can be approached in two ways: Closest Approach (CA), Encountered View (EW).

In the CA method, for every storm recorded within a 400 km radius of a port, the time of minimum geodesic distance (its closest point of approach) is identified. The storm is then assigned to a single category and ring based on the reported sustained wind at that time. CA produces a clean, one-storm-one-cell exposure matrix, making results directly comparable to previous studies (Flynn, 2023).

In the EW method, all storm fixes within 400 km window are considered, and the highest intensity category reached within that range is identified. Among the times corresponding to that highest category, the smallest ring is selected for classification. EW captures the storms whose peak intensity occurs before or after the closest pass and ties classification to the peak hazard state experienced in proximity. This mirrors established exposure datasets that categorize events by the peak sustained wind experienced at a site rather than solely by the distance at the CA (Geiger et al., 2018; FEMA, 2018).

In this study, both approaches are applied to develop a port-specific cyclone database for multiple purposes, including documenting past cyclone events within 400 km of the port, their frequencies, strike distances, and intensities. The distance from each cyclone fix to the seaport is calculated using the Vincenty formula, which determines geodesic distances on an ellipsoidal model of the Earth (Thomas and Featherstone, 2005). This method offers greater accuracy than spherical models, such as the haversine formula, as it accounts for the Earth's flattening and is widely used in geodesy.

Once the cyclones are classified and their corresponding frequencies and intensities are determined for the seaport, their impacts on port facilities, including critical equipment, are analysed to estimate the resulting functionality loss, as discussed in the following section.

3.2. Functionality loss assessment

3.2.1. Cyclone-induced damage states definition

Developed by the Federal Emergency Management Agency (FEMA, 2024b), the HAZUS Hurricane Model offers a standardized framework for estimating wind- and surge-induced damages across infrastructure systems. By defining consistent damage state taxonomies and fragility relationships, it provides a robust and adaptable basis for assessing cyclone-induced functional disruptions in seaport assets. Accordingly, this study adopts and tailors the four HAZUS damage states (DS), namely slight, moderate, extensive, and complete to evaluate cyclone impacts on port functionality, as follows (FEMA, 2024b):

DS1, or slight/cosmetic damage, involves non-load-bearing elements (cladding, signage, LED mast lights, CCTV housings, fender facings, paint, cable trays) being dented, shattered, or scoured by debris. Such superficial defects have no effect on throughput and can be repaired in parallel with more serious work.

When a cyclone moves to DS2, seaport structures remain sound, but their functionality is interrupted. Typical triggers include a tripped 11-kV substation, flooded fibre-optic rings, de-calibrated automated stacking cranes, or misaligned gate traffic-control masts. Throughput is curtailed until systems are reset or minor components replaced, usually a matter of hours to days. This state aligns with moderate label in HAZUS.

DS3 marks the threshold of localised structural failure, representing the extensive states in HAZUS. In this class, a quay crane boom

may collapse onto a vessel while the tower and sill beam survive; a rubber-tyred gantry's sheave housing may tear away; or a warehouse roof truss may partially uplift. The affected berth or yard is closed, and neighbouring assets operate under caution, with repairs typically stretching into weeks.

Finally, DS4 or complete damage, denotes major structural failure or near-total loss. Core load-carrying elements such as wharf decks, piles, or bollards suffer full-depth cracking, displacement, or pull-out. Crane overturning and progressive collapse of warehouse frames are also possible and expected. The berth might be out of service for weeks, often requiring redesign before reconstruction.

By coupling each damage state with clear operational consequences and indicative repair horizons, this approach provides a consistent basis for developing fragility curves, estimating downtime, and prioritising resilience investments at cyclone-exposed ports.

Prior to assigning DSs to individual port assets, it is essential to identify those whose failure would critically impair port functionality. Drawing on the Critical Path Method (CPM), a scheduling technique long employed in construction and recently recommended by the U.S. National Institute of Standards and Technology (NIST) for disaster-recovery modelling (Lavelle et al., 2020), an analogous concept is newly adopted for seaport operations in this study. Here, the critical path denotes the sequence of repair and restoration activities that constrains the earliest time at which a port can resume operations, given limited labour, and the technical precedence of tasks. Any delay along this chain postpones the port's overall reopening. Table 2 summarises the critical-path components developed from historical post-cyclone recovery records and the relevant literature.

3.2.2. Physical damage probability assessment

To estimate the probability of physical damage and potential downtime of seaport equipment caused by different types of cyclones, fragility curves are developed. A fragility curve addresses the following question:

> *"Given that the port is impacted by a wind speed of V, what is the probability that a structure reaches or exceeds a specific damage state (DS)?"*

In line with performance-based engineering practice and hurricane vulnerability studies, the port-asset fragility curve is modelled as a lognormal exceedance function (Li and Ellingwood 2006; Du and Hajjar 2024). Specifically, for damage state k,

$$F_{q,k}(v) = P[DS \geq k | V_{10} = v] = \Phi\left(\frac{lnv - ln\theta_{q,k}}{\beta_{q,k}}\right) \tag{1}$$

where,

$F_{q,k}(v)$ is the fragility curve for critical item q in the damage state k,

$\theta_{q,k}$ indicates the median resistance-wind at which there is a 50% chance of reaching DS $\geq$ k,

V_{10} denotes the 10-minute sustained wind at the quay,

$\beta_{q,k}$ represents the log-dispersion.

The lognormal form is standard as wind demand and capacity uncertainties are multiplicative and strictly positive, and it is the default in the FEMA fragility development guidance (FEMA 2020).

Having derived the fragility curves, the probability that each critical item q will fall into a given damage state k can be expressed as a Monte Carlo expectation (Li and Ellingwood 2006), as follows:

$$P_{q,k}(S) = E\left[F_{q,k}(v)/S\right] \tag{2}$$

$$S = (Ringzone[r_{min}, r_{max}], JMAclassC) \tag{3}$$

Here, S represents the cyclone type within the predefined ring zones boundary.

Table 2
Critical path items in a typical seaport.

Items	Descriptions	References
Navigation channels	Hydro surveys and debris clearance are prerequisites for reopening to vessel traffic; these activities control the initial restart.	(Touzinsky et al., 2018)
Quay/berth sub-structure (quay wall, relieving platform, rails)	A berth must be structurally sound and level before cranes can run or a vessel can moor. PIANC's Seismic Design Guidelines for Port Structures and ASCE/COPRI 61–14 both treat pile or gravity-wall failure as a "functional collapse" mode for the terminal.	(Association, 2002; Engineers, A. S. O. C., 2014)
Quay cranes	They are the only means to transfer containers between ship and shore; downtime directly halts throughput. Recent reliability studies rank quay cranes as the highest-critical asset class in container terminals.	(Rosca et al., 2025; Đelović, 2024)
High-voltage power supply (11–33 kV ring, main sub-station)	Modern quay cranes and many berth services are 100% electric. Loss of the ring or primary sub-station disables every crane simultaneously. The FEMA hurricane manual and multi-hazard risk assessments for ports flag electric power as a dominant single-point vulnerability.	(Verschuur et al., 2023; FEMA, 2024b)
Terminal backbone IT / SCADA node	After hurricane Sandy, submerged control rooms and servers kept otherwise undamaged terminals closed for weeks; the USCG Hurricane-Sandy after-action report lists TOS servers and fibre switches with the same priority as cranes and fuel jetties.	(Sturgis et al., 2014)

It should be noted that the translational speed of a cyclone's eyewall is not a reliable indicator of failure probability assessment. Instead, the wind speed experienced at a port serves as the primary criterion for assessment. To implement this, wind speed samples specific to the port must be obtained. To this end, the following steps are taken:

1) Cyclone track and wind data.

For each recorded cyclone, the centre position (at 6-hour intervals) and the official peak 10-minute mean wind speed (denoted as Vmax) are extracted.

2) Radius of maximum wind (RMW).

Since most storms lack an observed RMW, it is estimated using the climatological power-law–exponential relation of Trabing et al. (2024), which links RMW to storm intensity and latitude, as follows:

$$RMW = \alpha {V_{Max}}^{\beta} e^{\gamma * LAT} \tag{4}$$

where V_{MAX} is the maximum intensity in units of m/s, LAT is the latitude in degrees, and the coefficients are $\alpha = 671.3$, $\beta = -0.9516$, and $\gamma = 0.0242$.

3) The Holland parametric wind-field.

In the next step, the symmetric Holland vortex model is applied to calculate the gradient wind at any given radius r, corresponding to the port location (Holland 1980). This provides an estimate of the highest 10-minute mean wind speed that could have been experienced at the seaport during the cyclone's passage.

$$V_P(r) = K_m V_g(r) = k_m \sqrt{\frac{B\Delta P}{\rho}\left(\frac{R_m}{r}\right)^B e^{-\left(\frac{R_m}{r}\right)^B} + \frac{(f_r)^2}{4}} - \frac{f_r}{2} \tag{5}$$

where,

$V_P(r)$ is the estimated wind speed at port,

$V_g(r)$ is the gradient-level tangential wind at radius r from the cyclone centre,

k_m represents 10-min reduction factor at 10 m height,

B denotes Holland shape parameter (dimensionless), typically between 1–2,

ΔP is the sea-level pressure deficit,

ρ is the air density,

R_m is the radius of maximum wind (m),

f_r is the Coriolis parameter.

It should be noted that the adopted wind-field and cyclone modelling approach relies on several simplifying assumptions, which inevitably introduce some degree of uncertainty into the estimated wind speeds at the port location. First, the use of the symmetric Holland parametric wind-field model assumes an azimuthally uniform cyclone structure, thereby neglecting wind asymmetries arising from storm translation, environmental wind shear, and land-sea interactions. While this assumption is widely used in engineering-oriented hazard assessments and has been shown to provide reasonable first order estimates of cyclone wind fields, it may lead to an underestimation of peak winds on the right-hand side of the storm track and a corresponding overestimation elsewhere.

Second, as discussed earlier, the RMW is not directly observed for most historical cyclones and is therefore estimated using a climatological empirical relationship. Although the adopted formulation performs well on average for Western North Pacific storms, uncertainty persists at the level of individual events, particularly for cyclones undergoing rapid intensification or structural evolution.

Nevertheless, these uncertainties, which are inherent and unavoidable aspect of cyclone hazard modelling, are partially mitigated in the present study by adopting a probabilistic perspective. Specifically, the analysis relies on wind speed samples derived from multiple historical cyclone realizations rather than single-event deterministic estimates, thereby providing a more robust representation of wind hazard variability at the port scale.

By integrating fragility curves with the empirical wind speed samples described above, raw cyclone track data can be transformed into quantified estimates of functionality loss. This approach provides a consistent basis for assessing physical damage probabilities of critical equipment, estimating downtime, and prioritizing resilience investments at ports exposed to cyclones.

3.3. Economic loss assessment

Estimating economic losses in seaports exposed to tropical cyclones is a critical process that requires clear categorization of cost types and an understanding of their specific characteristics. Such losses can generally be grouped into three categories: direct damage costs, referring to physical damage to port equipment, infrastructure, and components; downtime costs, representing the economic impact of throughput loss due to service interruption or reduced operational capacity; and repair and recovery costs, encompassing expenses for restoring damaged assets and resuming normal operations. A comprehensive economic loss model should integrate all three components, with their respective contributions explicitly formulated to ensure accurate estimation of total losses. The following outlines each cost model in detail:

Direct damage costs can be estimated by assessing the probability of different DSs for each scenario and applying the corresponding loss ratios for those states, as follows:

$$C_{Pd} = \sum_{i=1}^{n} Q_i C_i \overline{d}_i \tag{6}$$

$$\overline{d}_i = \sum_{k=2}^{4} P_i^{DS_k} LR_i^{DS_k} \tag{7}$$

$$LR_i^{DS_k} = \frac{Replacementcostofasseti|DS_k}{Fullreplacementcostofasseti} \tag{8}$$

where,

C_{Pd} is the direct physical damage cost.

Q_i is the quantity of asset i (e.g. quay cranes, berths equipment, power system equipment).

C_i is the replacement or major-repair cost per unit of asset i.

$\overline{d}_i$ is the expected damage ratio for asset i.

$P_i^{DS_k}$ is the probability of damage state k for asset i.

$LR_i^{DS_k}$ is the mean loss ratio of asset i associated with damage state k.

The downtime costs can be broadly categorized into two components: throughput loss, and gale-force-induced operational stoppages. Throughput loss refers to the revenue shortfall resulting from a reduction in cargo handling capacity following a cyclone event. Gale-force stoppages occur when port operations are suspended due to high wind speeds, typically exceeding 35-40 knots, in compliance with safety regulations. During this time, all container-handling activities are stopped, leading to a complete halt in throughput.

$$C_T = (T^{intact} - T^{disrupted}) \times \rho \tag{9}$$

$$C_G = \frac{Hr_{gale}}{24} \times T_{daily}^{intact} \times \rho \tag{10}$$

where,

C_T represents the throughput revenue loss.

T^{intact} denotes the intact throughput (TEU).

$T^{disrupted}$ indicates the throughput after disruption (TEU).

ρ is the handling tariff or margin per TEU.

C_G is the gale-force stop cost.

Hr_{gale} represents the hours of sustained wind $\geq$ 35 kt at the quay.

In the recovery cost modelling process, costs are classified into two categories: time-sensitive and non-time-sensitive. Direct damage costs, which apply uniformly to equipment and assets requiring replacement, are fixed in nature and thus considered non-time sensitive. However, accelerable blocks, which are time-sensitive, include:

1) Crew and logistics labour (overtime, extra shifts),
2) Mobilization/demobilization and site setup (barges, temporary workshops, cranes),
3) Expedited parts and freight premiums (air freight, customs, courier),
4) Equipment rental and standby (mobile cranes, generators, IT trailers).

Time is critical for these items; delays or accelerated processes directly impact expenditure. Faster recovery can reduce overall downtime, which in turn minimizes revenue loss. This means that while immediate recovery efforts may appear costly, the long-term financial impact could be lower due to the quicker return to full operational capacity (Toğan and Eirgash, 2019). The balance between rapid recovery and cost efficiency is, therefore, a critical consideration for seaports.

The following formula outlines the developed approach for estimating recovery costs in seaport contexts:

$$C_{Rec} = \sum_i C_{Pd,i} + \sum_{i,k} \sum_{j \in J} B_{i,k}^{(j)} F_{i,k}^{(j)}(\alpha_{i,k}) \tag{11}$$

$$F_{i,k}^{(j)}(a_{i,k}) = \left(1 + \alpha_{i,k}^{(j)} \left(\gamma_{i,k}^{j} - 1\right)\right)^{b_{i,k}^{(j)}} \tag{12}$$

$$\gamma_{i,k}^{(j)} = \frac{T_{i,k}^{base}}{T_{i,k}^{acc}} \tag{13}$$

$$B_{i,k}^{(j)} = \begin{cases} \left(n_{i,k}^{int} w^{int} + n_{i,k}^{ext} w^{ext}\right) T_{i,k}^{base} (j = 1) \\ M_{i,k}^{mob} (j = 2) \\ E_{i,k}^{exp} (j = 3) \\ R_{i,k}^{rent} . T_{i,k}^{base} (j = 4) \end{cases} \quad (14)$$

where,

C_{Rec} is the recovery cost,

$C_{Pd,i}$ represents the replacement cost of component i,

$B_{i,k}^{(j)}$ is the baseline cost for accelerable blocks of class i in state k,

$F_{i,k}^{(j)}(\alpha_{i,k})$ denotes the time–compression premium,

$\gamma_{i,k}^{(j)}$ is the recovery duration ratio,

$a_{i,k}^{(j)}$ is the first-increment mark-up coefficient,

$b_{i,k}^{(j)}$ is the convexity (escalation) exponent,

$n_{i,k}^{int}$, w^{int} represent the in–house crew size and daily wage,

$n_{i,k}^{ext}$, w^{ext} represent the external crew size and daily wage,

T_{ik}^{base} is the baseline repair duration for component class i, DS_k (day).

$T_{i,k}^{acc}$ is the accelerated recovery duration for component class i, DS_k (day),

$M_{i,k}^{mob}$ denotes one–time mobilization/demobilization cost at normal speed,

$E_{i,k}^{exp}$ is the baseline expediting/freight cost,

$R_{i,k}^{rent}$ represents the daily rental rate of external equipment.

The parameter $\alpha_{i,k}^{(j)}$ represents the proportional cost premium incurred when the initial reduction in repair time occurs (i.e., when $\frac{T_{i,k}^{base}}{T_{i,k}^{acc}}$ is just above 1). It accounts for additional expenses such as overtime pay, night-shift differentials, expedited freight for spare parts, and standby-crew retainers. The parameter $b_{i,k}^{(j)}$ indicates how rapidly the cost slope steepens as repair time decreases. In other words, it governs the rate at which costs escalate as the repair process approaches its crash limit. If $b = 1$, the relationship between time and cost follows a linear trajectory. However, if $b > 1$, the curve becomes convex, meaning that each additional day of effort to reduce repair time incurs exponentially higher costs compared to the previous day. Together, these two parameters ($\alpha_{i,k}^{(j)}$, $b_{i,k}^{(j)}$) make the recovery cost model fully time-sensitive, transparent, and aligned with the time–cost trade-off objectives (Błaszczyk and Nowak, 2009; Hochbaum, 2016).

Regarding the relationship between the cost components and the need to avoid double counting, it is important to clarify that direct damage costs include the capital expenditures required to replace or permanently repair damaged equipment and infrastructure, including procurement, transportation, and installation of new assets. In contrast, recovery costs are limited to the expenses associated with restoration activities, such as maintenance operations, emergency repairs, overtime labour, and mobilisation of recovery resources, explicitly excluding the cost of new equipment, which is already accounted for within the direct damage cost component.

Accelerated recovery actions generally shorten the duration of system disruption and thus reduce downtime costs; however, such actions typically require higher recovery expenditures. In this formulation, downtime cost is treated as a dependent or follower cost component, determined after the recovery trajectory is established. Specifically, downtime cost is calculated by quantifying the cumulative throughput loss relative to the pre-event intact operational level over the disruption and recovery period.

Recovery costs, by contrast, are primarily governed by the resilience strategies adopted by the port, such as the allocation of additional repair crews, extended working hours, or the use of expedited maintenance procedures. Increasing investment in recovery activities raises recovery costs but reduces recovery time, thereby mitigating downtime losses. This unidirectional dependency, whereby recovery decisions influence downtime costs but not vice versa, is explicitly embedded in the formulation of the proposed cost model to ensure internal consistency and prevent double counting.

3.4. Terminal simulation modelling

3.4.1. Model structure learning

To model the terminal simulation, this study concentrates on the quay side, with a particular emphasis on berthing and cargo-handling operations. This is primarily due to the critical role of quay side as the interface between the maritime and landside domains, where complex coordination is required between large ocean-going vessels, quay cranes, and terminal transport systems (Hamka, 2017; Majumdar et al., 2022). The sheer scale of the vessels involved, combined with the high density of operational activities and time sensitivity of port calls, further amplifies the operational and safety–critical nature of this zone.

Given the operational and process-driven nature of container terminal activities, this study adopts discrete event simulation (DES)

over system dynamics (SD) and agent-based modelling (ABM). DES conceptualizes the system as interrelated processes and events (Karnon et al., 2012; Robinson, 2005), such as vessel arrival, container unloading by quay cranes, transport by AGVs or trucks, and yard storage or retrieval. By modelling events at discrete time points with explicit resource allocation and process flows, DES offers a realistic, structured approach to capturing terminal complexity. This makes it the most suitable method for developing a detailed, process-oriented simulation of container terminal operations.

To ensure the model is developed appropriately, a systematic and structured approach is adopted. This includes clearly identifying the input data, defining model assumptions, mapping the interactions between simulation entities, and determining the expected outputs. Fig. 3 presents the flowchart of quayside operations, highlighting each critical entity involved in the simulation as part of the modelled system.

As it can be seen, the simulation begins with vessel arrival, entering a queue based on schedules provided by shipping lines and terminal operators, ensuring realism compared to random arrivals. Berth allocation does not strictly follow First-Come-First-Served; factors such as service agreements, vessel size, and priority influence decisions. Vessels are classified by TEU capacity, length, draft, and other parameters to accurately model berth and crane allocation.

Berth assignment considers berth capacity, vessel dimensions, and safety checks before pilotage and mooring. Pilotage duration varies with vessel size, port layout, tides, and weather. After berthing, quay cranes are assigned based on vessel class, berth length, workload, and operational constraints, with large vessels potentially receiving six to eight cranes.

Container handling time depends on crane count, productivity, total containers, transport availability, and yard congestion. Departure preparation includes documentation, clearance, crane disconnection, and tug assistance if needed. Unberthing introduces additional delays. Once the vessel departs, berth and cranes are released for the next vessel.

This sequence of events constitutes the overall logical flowchart of the quayside simulation in a seaport, capturing the essential processes, resource dependencies, and operational dynamics involved in vessel handling. In line with best shipping practices, the simulation models three key delay types to represent operational inefficiencies and improve realism, with measurable impacts on overall throughput and vessel turnaround time (see Table 3). These delays are treated as influential variables and are systematically monitored and measured throughout the simulation period to assess their impact on terminal performance.

3.4.2. Model validation process

A multi-faceted validation approach is adopted in this study to ensure the reliability and robustness of the developed simulation model (Sargent, 2013), as follows:

1) Face validation: The model structure, flow logic, and operational assumptions are reviewed by academic and industry experts with experience in maritime logistics and port operations. Their feedback confirms that the simulation flow, including vessel arrival, berth allocation, crane operations, and container throughput processing reflect realistic port dynamics.
2) Literature-based parameter validation: Input parameters such as vessel inter-arrival times, quay crane efficiency, berth utilization, and vessel turnaround times are compared with the existing literature and port studies. The resulting outputs, such as average berth occupancy and crane usage rates, should be consistent with reported benchmarks for medium-to-large container ports.

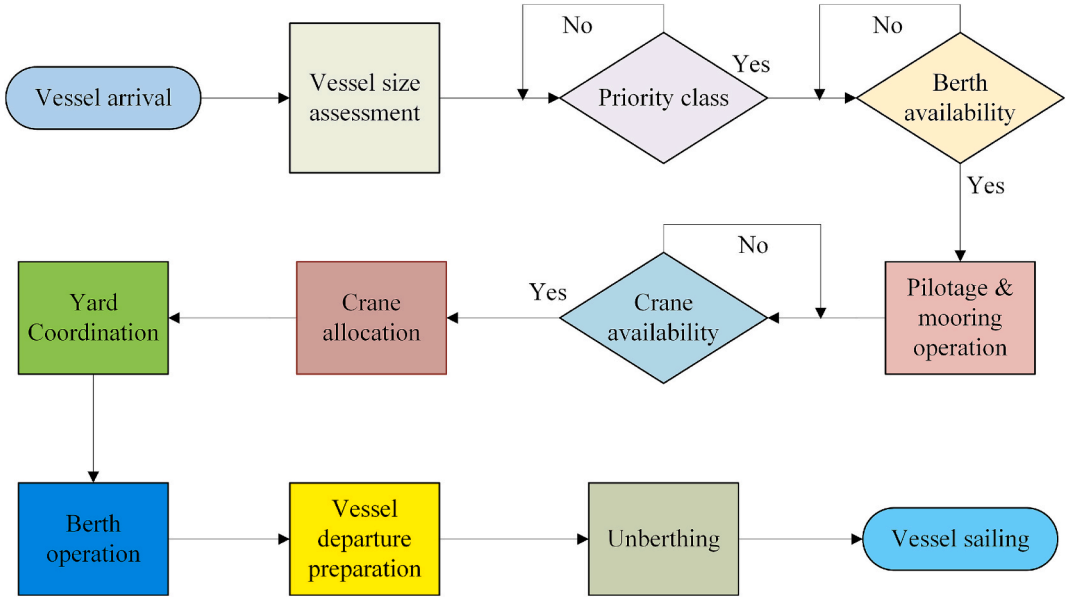

Fig. 3. Illustrative flowchart of quayside processes in a standard container terminal.

Table 3
Different types of delay in simulation logic.

Berthing Idle Time (t_{db})	Definition	The delay between the time a ship arrives at the port and the time it is assigned to a berth.
	Calculation	Berthing Idle Time = Time of Berthing – Time of Arrival
	Cause	Caused by berth unavailability due to congestion or priority rules and/or tidal effect.
Crane Allocation Idle Time (t_{dc})	Definition	The delay between the time a ship is berthed, and the time loading/unloading begins.
	Calculation	Crane Allocation Idle Time = Start Time of Operation – Time of Berthing
	Cause	Occurs when cranes are unavailable or occupied with other operations.
Unberthing and Clearance Time (t_{du})	Definition	The time between the end of the loading/unloading process and the ship's actual departure.
	Calculation	Unberthing Delay = Time of Departure – End of Berth Operation
	Cause	Caused by administrative, operational, physical and/or environmental (incl. tides) delays in releasing the ship.

3) Comparison with actual terminal records: The simulation output, such as the predicted throughput, container movements, vessel handling times, and cargo processing rates are rigorously compared against historical terminal operation records.
4) Sensitivity analysis: Key operational parameters, such as crane downtime, number of available berths, and different idle times are systematically varied to assess model responsiveness. Results should represent plausible system behaviour, such as proportional changes in throughput and recovery time, thereby confirming the model's internal consistency.

4. Case study

To demonstrate the applicability of the proposed framework, Kaohsiung Port, recognized as one of the world-leading and largest seaports and a principal transshipment hub in East Asia, was selected as the case study. Terminal 7, one of its most modern and busiest terminals, handles significant container volumes and features advanced infrastructure. Developed collaboratively by Evergreen Marine Corp. and Taiwan International Ports Corporation (TIPC), it features state-of-the-art automation technologies, including remote-controlled quay cranes, unmanned rail-mounted gantry cranes, and integrated AI-driven systems. The choice of this modern container terminal is also for the result generality given the high standardisation of container terminals compared to the others. Its strategic location and high exposure to typhoons make it an ideal case for simulating cyclone impacts and assessing vulnerability in a real-world, high-risk operational environment. Table 4 presents technical details of Terminal 7 at Kaohsiung Port.

4.1. Data collection of terminal operation

Operational data were collected from Terminal 7 records covering a year period from 1 August 2024 to 31 July 2025. The dataset includes key information such as vessel name, arrival time, berthing time, operational time, and departure time. The collected data were systematically processed to classify vessels by size and estimate the number of containers to be loaded and unloaded. As shown in Fig. 4, more than 2010 vessels visited the terminal during the study period, with the majority classified as feedermax vessels.

Based on the collected data, for each vessel category, key operational time components were analysed in detail: berthing time (which includes the time required for pilotage and mooring), crane allocation time (the time it takes for the cranes to set up for the operation), operation time (the duration needed for loading and unloading containers), departure time (the time allocated for vessel preparation before leaving the terminal) and finally the turnaround time (the time between the vessel arrival and departure). Probability distributions were fitted to each category based on observed patterns, enabling an accurate characterization of their time behaviour. To obtain these statistical distributions, first, extreme observations were removed because vessel-time data occasionally include key-entry errors or very rare events that distort goodness-of-fit tests. The resulting samples retained more than 95% of the

Table 4
Technical information of Terminal 7 at Kaohsiung port (Port Technology International 2024).

Entity	Description
Terminal 7	Geographical Area: Located in Kaohsiung, Taiwan: Latitude: 22.560112° N Longitude: 120.331185° ETotal Area: Approximately 149 ha.
Throughput	Annual: Current capacity of 4.5 million TEUs, with planned enhancements to reach 6.5 million TEUs. Monthly: Approximately with the capacity of 375,000 TEUs.Daily: Approximately with the capacity of 12,300 TEUs.
Berths	Number of Berths: 5 deep-water berths (S1-S5). Berth Capacity: Capable of accommodating up to four 24,000 TEU ultra-large container ships and two feeder vessels simultaneously. Draft: 18 m.Length: Total quay length of 2,415 m.
Quay crane	Automated: 19 out of 24 quay gantry cranes are remote-controlled. Speed: Each crane can handle 30–45 moves per hour. Capacity: Each crane can handle 25 rows of containers on deck.
Electrical station	Equipped with a dedicated substation supporting full electrification of terminal operations, ensuring a peak power demand of approximately 10 megawatts.
IT services	Utilizes Evergreen's intelligent terminal operating system (EMCTOS), integrating 5G communication systems, optical fibre connectivity, Internet of Things (IoT) networks, Optical Character Recognition (OCR) technology, and real-time power consumption monitoring to enhance operational efficiency

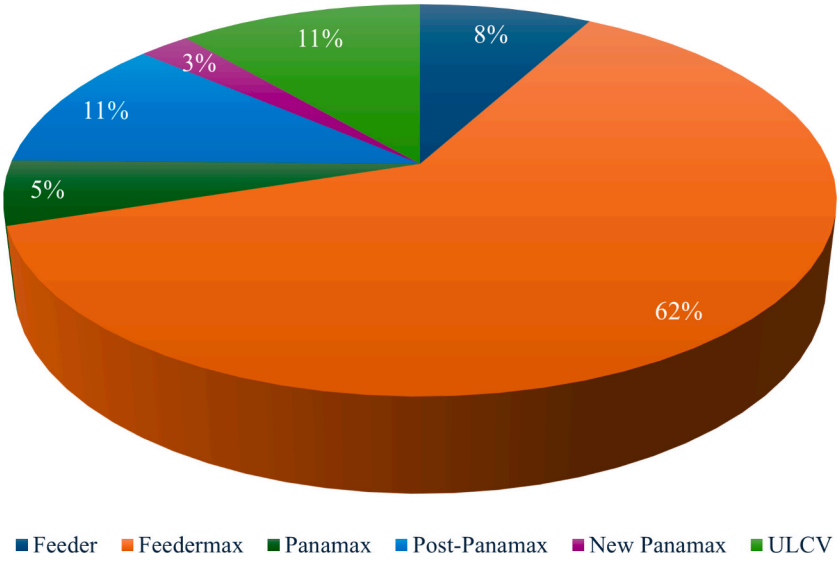

Fig. 4. Distribution of vessel types visiting terminal 7 from August 2024 to August 2025.

original records, so the fitted models still describe typical behaviour while allowing the most extreme outliers to be treated separately. The cleaned data were then fitted to several standard duration distributions (Log-normal, Gamma, Inverse-Gaussian, and Weibull). Parameters were estimated by maximum likelihood technique. Table 5 presents the statistical distribution summary derived from the collected data for various types of vessels that called at Terminal 7.

4.2. Simulation model of terminal 7

The berth layout at Terminal 7 is designed to accommodate four ultra-large 24,000 TEU container vessels (ULCV) alongside while still providing space for two feeder vessels, an arrangement enabled by dividing the central berth into sub-positions S3A and S3B. In fact, the first construction phase opened with Berths S5, S4 and S3B, while Berths S1, S2 and the companion S3A came on-line in the second phase, as illustrated in Fig. 5. To capture that physical layout, the AnyLogic DES model begins with the Excel-driven "Source block" that reads the real vessel schedule. Each spreadsheet row spawns a "Ship agent" carrying its call-size, class and the time of its arrival.

Newly created ships flow into an anchorage modelled by a "Wait block" whose release condition is the Boolean function "isBerthAvailable()". "Wait block" was chosen instead of a simple Queue because it can listen for a logical expression and wake all waiting entities the moment any berth becomes available.

Routing is handled by a five-exit "SelectOutput". The block evaluates berths in priority order but contains a short Java snippet that treats Berth 3 as two 285-m "slots".

The model then simulates the loading and unloading process. A "Seize block" taps a common resource pool of 24 quay crane units. The quantity expression "agent.nQCrequested" allows different vessels to request an appropriate number of cranes, as defined by a predefined distribution *(*Yu et al. 2024; Quist et al. 2021*)*.

Quayside work itself happens inside a "Delay block" whose duration is computed as follows:

$$Delaytime(Hour) = \frac{Containerquantity}{numberofcranes \times craneefficiency(MPH)} \tag{15}$$

where crane efficiency refers to the number of containers a crane can process per hour (moves per hour).

When loading and unloading finish, a "Release block" returns the cranes, and the ship enters a brief customs/clearance "Delay". At its end, a final "Release" frees the berth resource and flips the Boolean that will unblock the next waiting arrival. The agent then leaves through a "Sink" block.

Throughout the simulation, each resource pool, such as berths and cranes, maintains its own utilization statistics, while the timing blocks generate datasets that record ship turnaround times, berth throughput, and crane occupancy histories.

4.3. Simulation model validation

To validate the model more thoroughly, the multi-faceted validation approach introduced in Section 3.4.2 was applied. Firstly, as part of the face validation technique, the simulation model was presented to five experts with over 10 years of experience in seaport operations (Table A, Appendix). All the experts unanimously confirmed the logical accuracy of the model from vessel arrival through to

Table 5
Statistical distribution for different types of vessels.

Vessel type	Berthing time (hr.)	Crane allocation time (hr.)	Operation time (hr.)	Departure time (hr.)	Turnaround time (hr.)
Feeder	Inverse-Gaussian ($\mu = 2.74$, Scale = 1.214) + 0.4	Weibull ($k = 1.92$, $\lambda = 1.104$) + 0.35	Weibull ($k = 2.036$, $\lambda = 17.094$) + 1.95	Gamma ($k = 2.288$, $\theta = 0.369$) + 0.3	Gamma ($k = 4.289$, $\theta = 5.445$)
Feedermax	Inverse-Gaussian ($\mu = 5.239$, Scale = 1.159) + 0.5	Weibull ($k = 2.881$, $\lambda = 1.332$) + 0.4	Gamma ($k = 4.282$, $\theta = 4.622$) + 2.0	Lognormal (μ = -0.127, σ = 0.573) + 0.2	Inverse-Gaussian ($\mu = 0.26$, Scale = 115.987) + 2
Panamax	Inverse-Gaussian ($\mu = 2.082$, Scale = 1.445) + 0.4	Lognormal ($\mu = 0.101$, $\sigma = 0.376$) + 0.45	Inverse-Gaussian ($\mu = 0.126$, Scale = 155.932)	Lognormal ($\mu = 0.108$, $\sigma = 0.364$)	Inverse-Gaussian ($\mu = 0.124$, Scale = 210.64)
Post-Panamax	Inverse-Gaussian ($\mu = 5.651$, Scale = 1.298) + 0.55	Weibull ($k = 2.405$, $\lambda = 1.25$) + 0.4	Gamma ($k = 7.052$, $\theta = 2.991$)	Lognormal (μ = -0.05, $\sigma = 0.529$) + 0.25	Inverse-Gaussian ($\mu = 0.202$, Scale = 161.357)
New Panamax	Inverse-Gaussian ($\mu = 6.877$, Scale = 1.438) + 0.6	Inverse-Gaussian ($\mu = 0.047$, Scale = 31.244)	Weibull ($k = 2.996$, $\lambda = 43.597$)	Gamma ($k = 15.905$, $\theta = 0.095$)	Inverse-Gaussian ($\mu = 0.228$, Scale = 240.341)
ULCV	Inverse-Gaussian ($\mu = 4.765$, Scale = 1.177) + 0.5	Gamma ($k = 9.614$, $\theta = 0.164$)	Gamma ($k = 4.657$, $\theta = 6.846$)	Lognormal ($\mu = 0.313$, $\sigma = 0.331$)	Inverse-Gaussian ($\mu = 0.229$, Scale = 182.853)

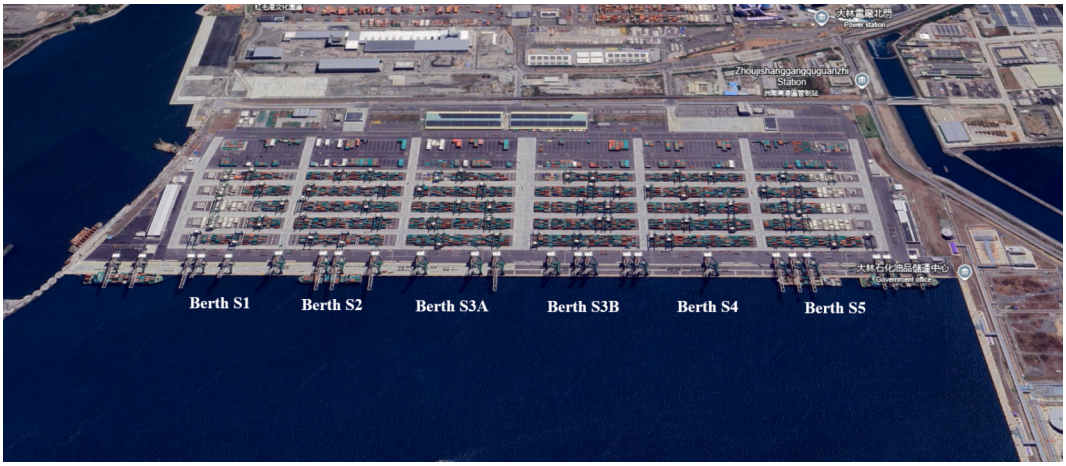

Fig. 5. Berth layout at Kaohsiung Port Terminal 7.

departure. Minor adjustments were suggested regarding berthing idle time and berth allocation rules, which were subsequently implemented in the model. Additionally, the logic for crane allocation, including the flexibility to share cranes between neighbouring berths was reviewed and enhanced based on experts' feedback. These refinements were incorporated into the final version of the model to ensure a more accurate representation of real-world operations.

From a literature perspective, the most critical parameters used in the developed simulation model were cross-checked against corresponding values reported in the literature for similar ports. As shown in Table 6, these parameters are consistent with values commonly found in previous studies, reinforcing the credibility and reliability of the inputs used in the model. This consistency indicates that the parameter selection is well-founded and that the model reflects realistic port operations. Consequently, the outputs generated by the simulation can be considered valid and aligned with established benchmarks in the field.

Based on real data collected from Terminal 7 and their integration into the developed simulation model, the output results are obtained and presented in Table 7. The model is initially run under normal operational conditions using the actual data. As shown, the simulated throughput closely matches the actual throughput of Terminal 7, with a minor deviation of 0.1%, which falls within an excellent margin of error. Additionally, the number of vessels that visited the terminal during the study period perfectly aligns with the number recorded in the operational logs, further confirming the reliability of the input data and model behaviour. Moreover, the average turnaround duration for all types of vessels visiting the terminal is comparable, with only a small, acceptable difference when compared to the average of the actual records.

Finally, the last validation technique applied was sensitivity analysis. The three most critical variables in the simulation model were selected for this purpose. As shown in Table 8, two different values, one below and one above the baseline, were chosen for each selected variable. The model was then run separately for each scenario to observe its response to changes in individual parameter values. It should be noted that the analysis period covers only a month of the whole collected data, allowing the model flexibility to account for fluctuations in logistics and throughput levels. The results of these simulations are presented in Figs. 6-8. It is evident that the model exhibits proportional behaviour in terms of quay crane utilization rate, level of throughput, and the number of vessels it processes. As the values of the critical variables increase or decrease, these variables' levels correspondingly rise or fall. This response confirms the logical consistency and robustness of the model, demonstrating that it reacts appropriately to changes in key operational inputs.

From a practical perspective, the sensitivity analysis offers clear and actionable insights for port managers by highlighting where interventions are likely to deliver the greatest benefits. The results show that the number of berths has the highest marginal sensitivity across all key performance indicators, including crane utilisation, terminal throughput, and the number of vessels served. For instance, adding a single berth can increase monthly throughput by at least 6,000 TEU under the same logistics configuration and crane fleet. In

Table 6
Parameter validation through literature review.

Parameter	Simulated model	Literature range	References
Vessel inter-arrival time (h)	4–8	3–10	(Pellemans et al., 2025; Saber et al., 2025)
Average berth utilization (%)	67	60–85	(Notteboom et al., 2021)
Average Vessel turnaround time (h)	26.2	20–35	(Notteboom et al., 2021)
Quay crane productivity (MPH)	30–40	25–45	(Achterkamp, 2019)
Average daily throughput (TEU)	8500	7000–12000	(Choi et al., 2022)
Average pilotage and mooring duration (h)	1.5	0.5–2	(Wu et al., 2020; Kasm et al., 2021)
Average crane allocation duration (h)	1.6	0.5–2	(Al-Dhaheri et al., 2016; Bierwirth and Meisel, 2010)
Average clearance and departure process duration (h)	1.5	1–3	(International Taskforce, 2019)

Table 7
Simulation model output under normal operation.

Items	Actual data	Simulation data	Accuracy rate (%)
Container throughput (TEU)	3,651,186	3,647,709	99.9
Number of vessels	2014	2010	99.8
Average turnaround (Hour)	27.3	26.2	95.9

Table 8
Sensitivity analysis logic.

#	Sensitivity Scenario (SS)	Low	Base	High
SS1	Number of quay cranes	19	24	29
SS2	Quay crane efficiency (MPH)	25–35	30–40	35–45
SS3	Number of berths	4	5	6

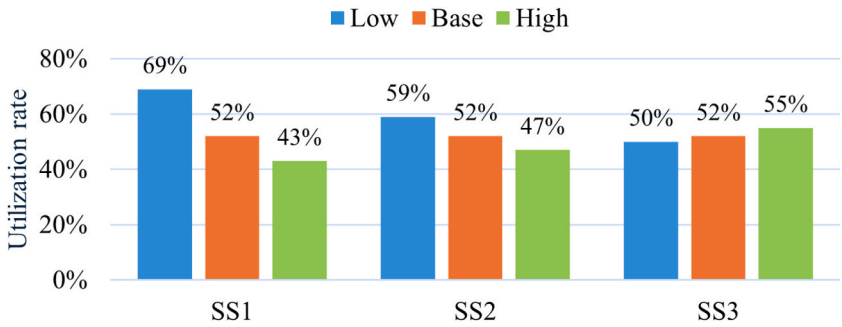

Fig. 6. Sensitivity analysis based on crane utilization rate.

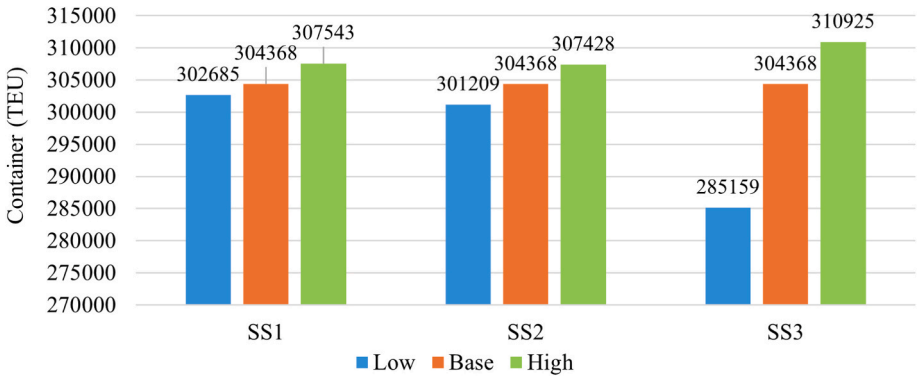

Fig. 7. Sensitivity analysis based on terminal throughput.

contrast, the loss of one berth leads to a throughput reduction of approximately 19,000 TEU over the same period.

This asymmetry underlines the critical role of berth availability and demonstrates that infrastructure-intensive investments, such as berth expansion, can generate substantial operational gains, provided that they are supported by adequate crane resources and efficient operations.

A similar sensitivity pattern is observed for the number of quay cranes and their operational efficiency, expressed in moves per hour (MPH). While increasing crane availability enhances overall throughput and vessel handling capacity, improvements in crane efficiency directly increase the quay service rate, with immediate effects on vessel turnaround time and berth occupancy.

Overall, the findings suggest that improving operational efficiency and actively managing crane availability provide effective levers for sustaining throughput and alleviating congestion. At the same time, the availability of structural assets, particularly berths, plays a dominant role during periods of disruption or partial system degradation, exerting a disproportionate influence on overall terminal performance.

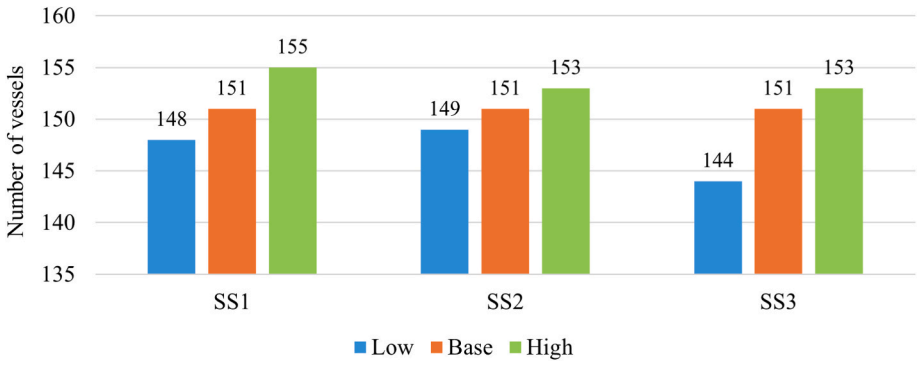

Fig. 8. Sensitivity analysis based on the number of vessels.

4.4. Tropical cyclones data collection and processing

In this study, the International Best Track Archive for Climate Stewardship (IBTrACS) database was used alongside the Typhoon Database Web Tool provided by the Central Weather Administration (CWA) of Taiwan (https://rdc28.cwa.gov.tw/TDB/public/typhoon_list) to identify and extract all tropical cyclones that have affected Kaohsiung Port over the past 30 years. The selected 30-year timeframe (1995–2024) was chosen to enable a comprehensive and long-term assessment of historical cyclone activity, thereby facilitating a clearer understanding of the potential frequency and impact of such events in the future. For each recorded cyclone, the centre position (at six-hour intervals) and the official peak 10-minute mean wind speed (V_{max}) were extracted.

Results indicate that 182 cyclones, irrespective of intensity or ring zone, passed within 400 km of Kaohsiung Port. Occurrence is strongly seasonal, peaking in July-August due to Kaohsiung's proximity to the highly active mid-summer Luzon Strait storm corridor, then declining in September as many tracks recurve northward and move away from Taiwan (Xue et al. 2023). The filtered cyclones, from both temporal and spatial perspectives, were derived using the CA and EW approaches and are illustrated in Figs. 9-10. Among storms with wind assignment at their CA approach ring, Typhoon-class cases account for 34.5% overall. At very close range (≤100 km) that share drops to 16.7%; whereas within 0–200 km it rises to 29.2%. In practice, direct eyewall-strength conditions at the port are uncommon, suggesting that most close CA events are Tropical Depression (TD), TS (Tropical Storm), and STS (Severe Tropical Storm) at the port. Under the EW approach, high-end exposure in the Typhoon-class is most common in the 150–300 km belt. Even when the closest pass is not near the port, the outer wind field can still drive gales, and operational slowdowns. EW approach is therefore the appropriate lens for ring-based triggers (e.g., crane derating, berth limits) tied to distance thresholds.

4.5. Development of fragility curves

To estimate the probability of cyclone-induced damage states, fragility curves are developed. Quay cranes are pivotal to terminal operations and particularly susceptible to high winds due to their height, structural complexity, and exposed components. Accordingly, parameter values for the lognormal fragility functions were derived from published technical documents and relevant case

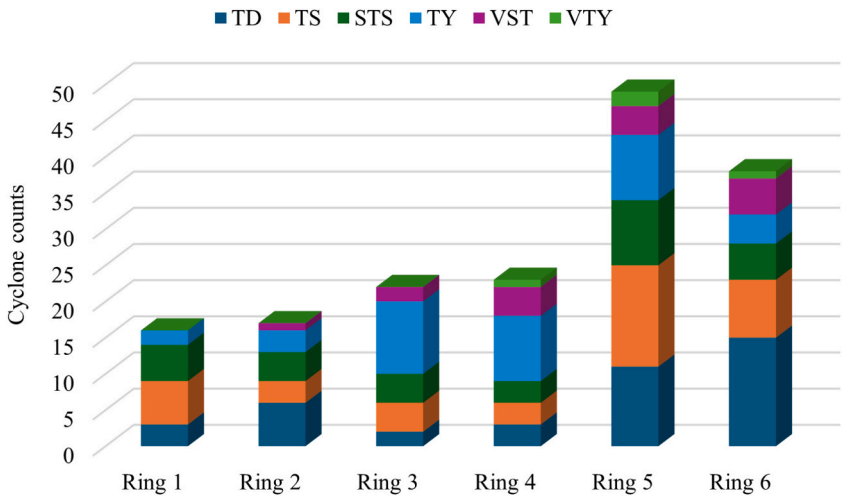

Fig. 9. The recorded cyclones in different distance rings based on CA approach.

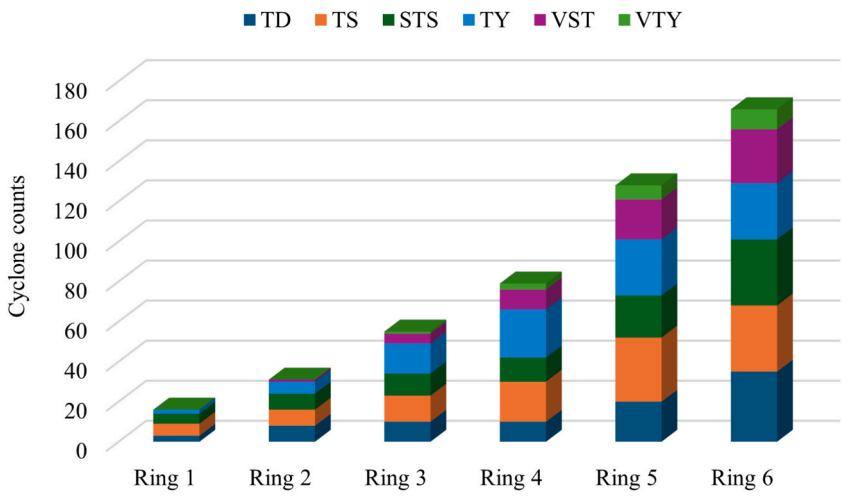

Fig. 10. The recorded cyclones in different distance rings based on EW approach.

studies. Table 9 summarises the adopted values and their justifications, and Fig. 11 presents the resulting fragility curves for all quay-crane damage states.

The median resistance (θ) and lognormal dispersion (β), which govern the shape and position of the fragility curves, were not chosen as isolated point estimates. Instead, they were informed by multiple, complementary sources of evidence, including OEM technical specifications, PEMA datasheets, international standards and port engineering guidelines, as well as documented case studies of wind-induced damage to quay cranes. To improve transparency, the objective basis for each damage state has been mentioned in Table 9, explicitly linking the selected parameter values to operational wind thresholds, design wind limits, and observed failure mechanisms. This approach ensures a clear and traceable connection between the physical behaviour of quay cranes and their probabilistic representation in the fragility model.

Building on the justification provided in Table 9, the selected median wind speeds (θ) were calibrated to reflect the onset of the dominant damage mechanisms associated with each damage state, rather than relying solely on regulatory or operational limits. For the lower damage states (DS1-DS2), the median values are intentionally positioned above shutdown thresholds so that the curves capture the emergence of minor and moderate physical damage, without confusing these effects with purely procedural or safety-driven stoppages.

Table 9
The quay crane fragility parameters.

Damage state	θ (m/s)	β	Objective basis	Reference
DS1	25	0.30	Minor, non-structural effects are expected a bit above the operational stop. The "gale" begins 17–19 m/s, where slight non-structural damage first appears; choosing 25 m/s centers DS1 above the near-gale band (no throughput impact).	(European Committee for Standardization (CEN), 2014; Konecranes., 2024; Cranes, 2025; PEMA, 2019Konecranes, 2021; Wu et al., 2022; McCarthy et al., 2009; Kim et al., 2004; Lee and Kang, 2008; Kang and Lee, 2008; Han and Han, 2011; Hoite et al., 2018; Bhimani and Soderberg, 2006)
DS2	30	0.30	Operational cut-off for quay cranes handling is consistently 18–22 m/s mean; PEMA (Port Equipment Manufacturers Association) recommends 18–19 m/s and OEMs (Original Equipment Manufacturer) list 20 m/s "in-service" wind. DS2 Makes moderate physical damage clearly higher than DS1 and comfortably below stowed design winds, hence the median is set at 30 m/s quite above the tight 18–20 m/s band.	
DS3	50	0.30	OEM out-of-service/stowed design winds bracket 42–60 m/s (e.g., Liebherr at 42 m/s, and Konecranes at 60 m/s). Case histories (e.g., Typhoon Maemi crane failures) also occur in this band. Picking 50 m/s places the median slightly above the lower OEM design value to represent the onset of localised structural failures across different designs/sites.	
DS4	60	0.30	DS4 is Governed by tie-down exceedance. Liftech recommends rare-event criteria: 7% in 50 yr for cranes, 3% in 50 yr for tie-downs. Taiwan typhoon extremes for 10-min means span 48–76 m/s across RP bands, and OEM lists 60 m/s stowed. Setting $\theta = 60$ m/s centers DS4 within the credible collapse/overturning range.	

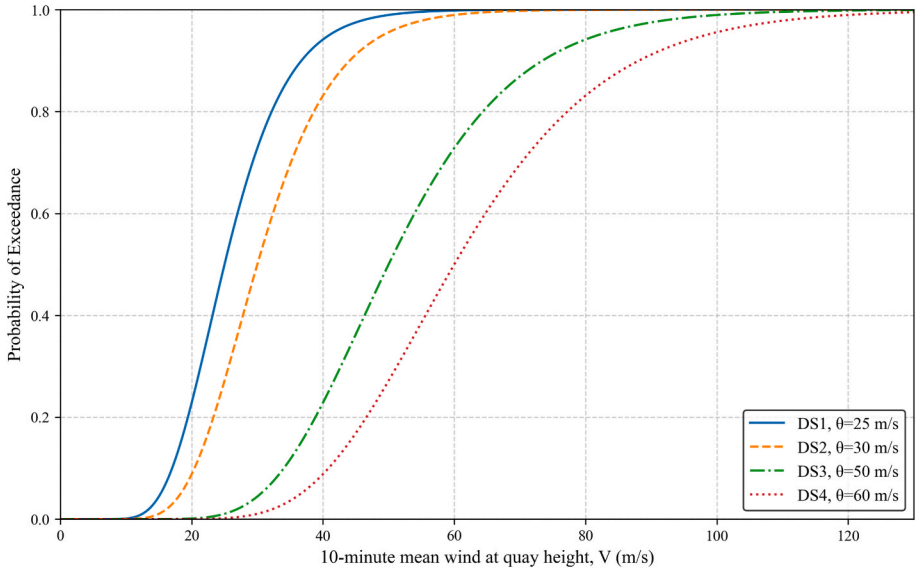

Fig. 11. The developed fragility curves for quay cranes.

Higher damage states (DS3-DS4) are anchored within the out-of-service and tie-down exceedance wind ranges reported by OEMs and historical cyclone-induced failures (e.g. crane collapses under typhoon conditions). This approach ensures that each θ value corresponds to a physically meaningful transition in structural response rather than a conservative or optimistic bound.

The dispersion parameter ($\beta = 0.30$) was chosen to reflect the natural variability across quay-crane designs, foundation conditions, maintenance levels, and local wind-field characteristics. This value is consistent with those commonly used in wind- and earthquake-related fragility studies of port infrastructure. Instead of assuming a narrow uncertainty band, a moderate level of dispersion was deliberately retained to avoid implying an unrealistic degree of precision, particularly given the absence of site-specific structural testing data.

As shown in Fig. 11, all curves exhibit the characteristic sigmoidal form of cumulative distribution functions, which indicate near-zero probabilities at low wind speeds, a rapid transition zone, and saturation near unity. DS1 displays a relatively broad transition, reflecting failure of minor attachments and cladding over a range of winds. DS2 also follows a similar trend, consistent with a procedure-driven operational shutdown; once winds approach the in-service limit, exceedance probability increases rapidly. DS3 initiates at substantially higher winds, consistent with the onset of damage to stowed cranes near or above the lower bound of out-of-service design winds, particularly under adverse configurations. DS4 is the rarest port shutdown state, triggered when extreme winds exceed the tie-down capacity of cranes. Although a tail event, its risk remains material for cyclone-exposed ports.

To characterise fragility-parameter uncertainty and assess model robustness, a sensitivity analysis was performed. The perturbations were applied to the lognormal fragility parameters for each DS, and the results are shown in Figs. 12-13.

Varying the median θ translates each curve horizontally without changing its shape. By construction, a 10% increase in θ shifts the 50% exceedance wind towards the higher speeds. This behaviour is evident in Fig. 12, where each damage state's baseline is bracketed by the $\pm$ 10% θ curves.

Varying the dispersion β affects only the transition width, in a way that larger β flattens the curve, smaller β steepens it. Quantitatively, the 10–90% transition ratio equals $\exp(2.563\,\beta)$. Thus, as an example, DS4 ($\beta = 0.25$) spans nearly 1.9 times the wind speed between the 10% and 90% exceedance points, whereas DS4 ($\beta = 0.30$) spans approximately 2.2 times the wind speed.

Within the Kaohsiung wind range, the higher damage states (DS3-DS4) are more sensitive to both parameter types than lower damage states, because DS1-DS2 are essentially saturated (exceedance$\approx$1.0) at $V_{10} \approx 50$ m/s, so local parameter variations have minimal effect.

It is to be noted that under a cyclone-wind-only scope and the quayside of the terminal, the only critical-path asset for which four structural damage states can be credibly defined and parameterised is the quay cranes. For the other items on the critical path, either hydrodynamic actions (surge, waves, currents, inundation) dominate physical damage, or the governing mechanism is administrative closure rather than structural failure. As a result, a wind-damage fragility curve development for those assets would therefore be physically misleading. Accordingly, we model each non-quay crane item as a functional node driven by a wind-triggered unavailability event and a restoration-time distribution followed by (Pianc, 2020; FEMA, 2024b).

4.6. *Component restoration curves development*

The expected downtime for each damage state is expressed as a baseline mean time to recovery (MTTR). This baseline represents standard operating conditions: normal spare-parts availability; at least one heavy-lift contractor on call; no prearranged mutual-aid

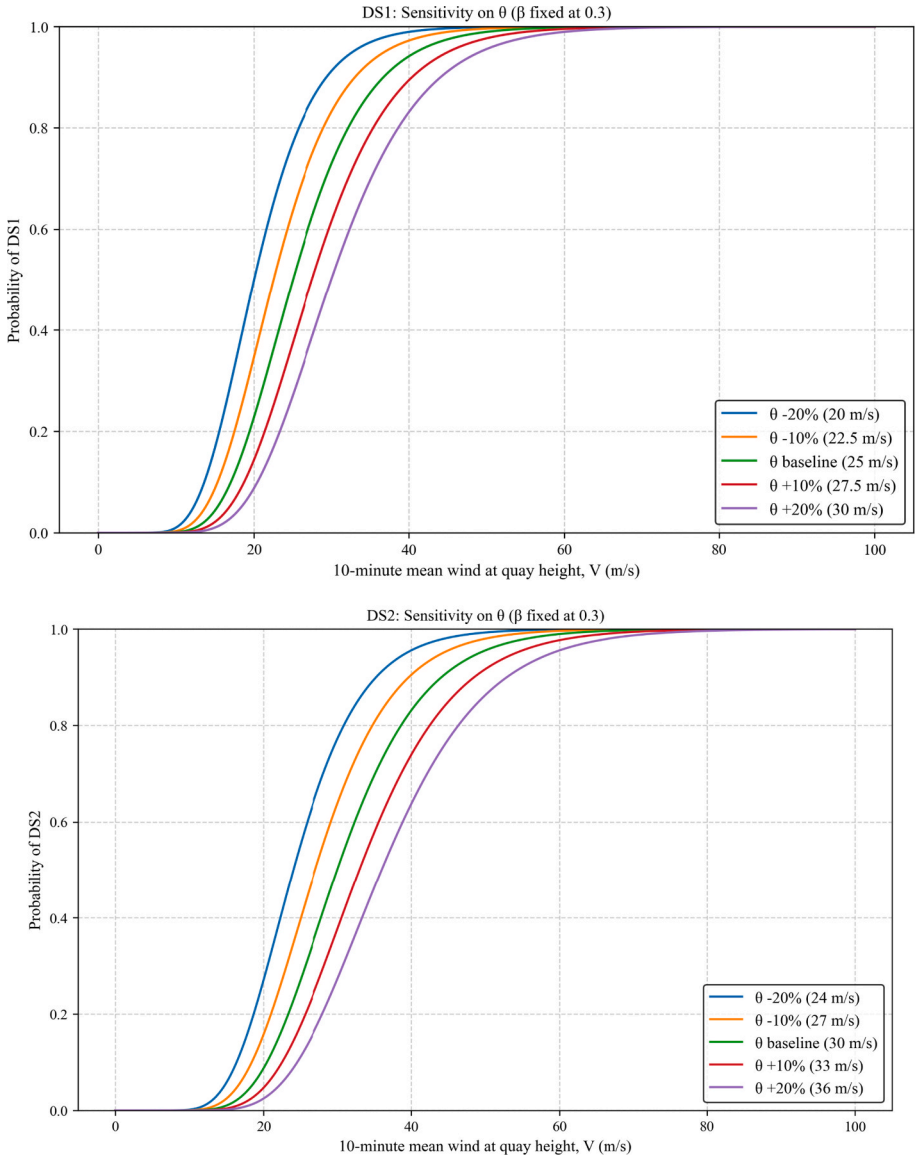

Fig. 12. Sensitivity analysis of fragility curves with respect to parameter θ.

cranes; and repairs performed during regular weekday working hours. This scenario aligns with what USACE (USACE 2019) define as a "Tier-2, standard-practice" port. Deviations from this baseline, whether due to better preparedness or more constrained conditions, will generally cause downtime to scale down and up, respectively.

Recovery durations are usually provided as realistic ranges, reflecting the inherent uncertainty due to varying parameters such as event intensity, cascading effects, preparedness, budget constraints, and severity of damage consequences. Rather than exact values, ranges offer a better practical understanding of potential downtime. For this reason, the restoration curves were developed using the HAZUS restoration functions for port system components, modelled as normal distributions (FEMA 2024a). The means and standard deviations of these functions as well as the discretized restoration probabilities are provided in Table 10, and Fig. 14 presents the corresponding restoration curves for all damage states.

As shown in Fig. 14, the HAZUS-based restoration curves convert uncertainty into time-bound probabilities of recovery. These curves are modelled as cumulative distribution functions, using the specified means and dispersions to yield percentile restoration dates. For quay cranes, a unit in DS2 has a 75% probability of being restored within 10 days, reflecting primarily repairable mechanical/electrical faults and limited structural remediation. DS3 requires more extensive interventions, including component replacement, alignment, and testing, so the probability of recovery reaches 84% only by about two months. DS4 represents toppling or near-total structural failure; recovery is dominated by procurement and installation of a replacement crane, permitting, and specialised

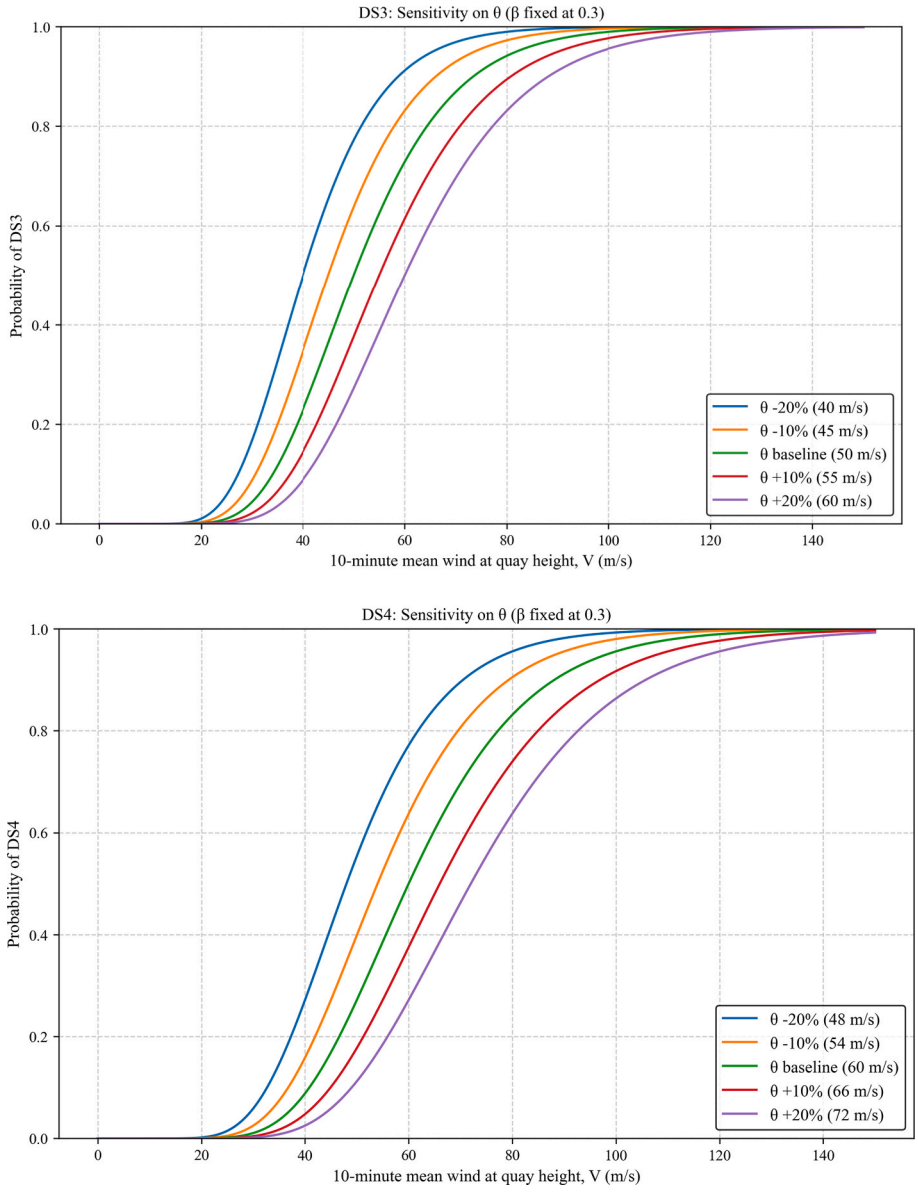

Fig. 12. (*continued*).

contractor availability. The whole process may even exceed a year.

5. Results and discussion

5.1. Terminal throughput loss estimation

Building on the damage state probabilities derived from the fragility curves, the potential quantities of failed quay cranes are estimated for each damage state. These estimates serve as key inputs for the simulation model used to assess potential throughput disruptions.

Damage-state probabilities are propagated into the simulation as capacity reductions and temporary closures. For each scenario the model reports processed throughput, the loss ratio (lost throughput/intact throughput), and the number of vessels diverted. Rerouting follows a transparent policy, as follows: if the port is closed, new arrivals are diverted; if open, any vessel whose expected waiting time exceeds a maximum tolerable wait is diverted to neighbouring ports through a “sink” module. This policy reflects industry practice that diversion is a conditions-based decision rather than a fixed standard, while preventing unrealistic queue build-up under degraded capacity (IMO 2021). It is important to note that the recovery process in all simulations is based on a baseline recovery policy,

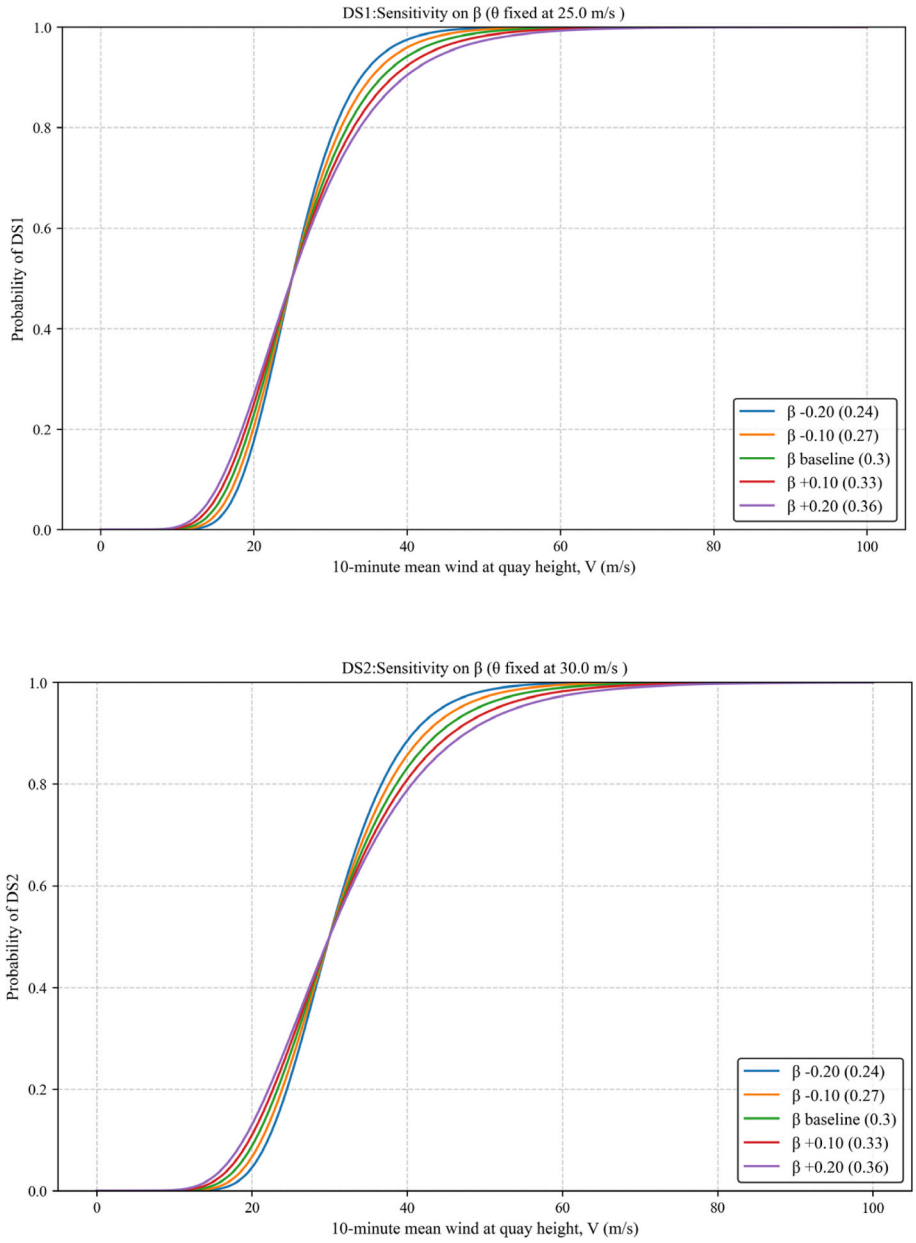

Fig. 13. Sensitivity analysis of fragility curves with respect to parameter β.

commonly referred to as the standard recovery approach, which represents typical or average post-disaster restoration conditions. These results are summarized in Table 11 and Fig. 15 shows the throughput loss under different scenarios within the specified ring zones.

As it can be seen, across all cyclone classes, throughput loss decays with distance from the terminal. Within Ring zone 1 (0–50 km), the throughput loss is the largest, especially under VTY conditions, while losses drop sharply under TS/STS scenarios and are the most negligible by Rings 4–6 (200–400 km). Only the VTY case retains a small but measurable loss at Ring 6 (~0.11%). This pattern is also mirrored in rerouting counts, which decreases monotonically with distance. The processed throughput correspondingly approaches the intact reference as distance increases.

These gradients indicate that hazard intensity and footprint scale with cyclone classes. The stronger cyclones degrade capacity, and thus increase the expected waiting times, far beyond the immediate vicinity of the port, and sustaining both higher loss ratios and more diverted vessels across multiple rings. Conversely, weaker storms primarily affect the inner rings only. The alignment between loss ratio, processed TEU, and rerouted vessels confirms that the rerouting policy is behaving as intended. It prevents queue blow-ups near

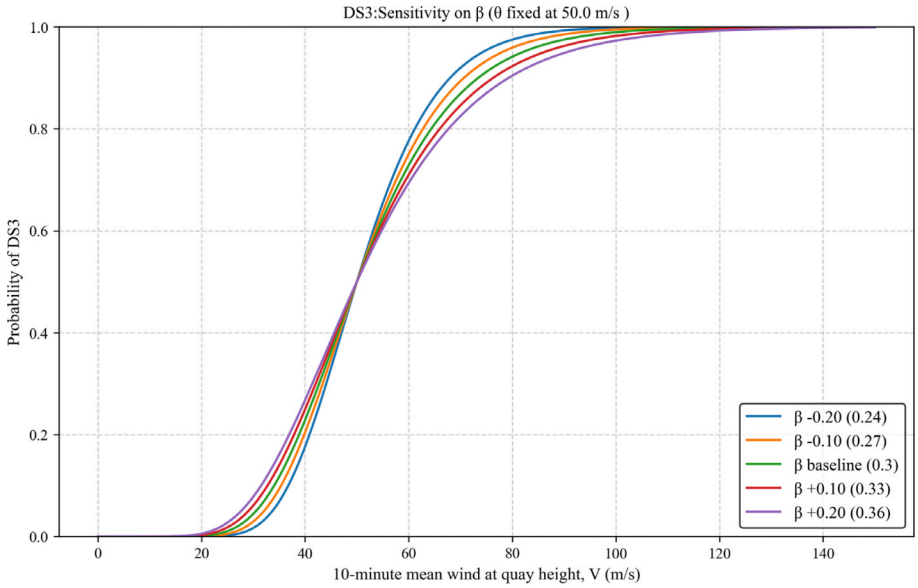

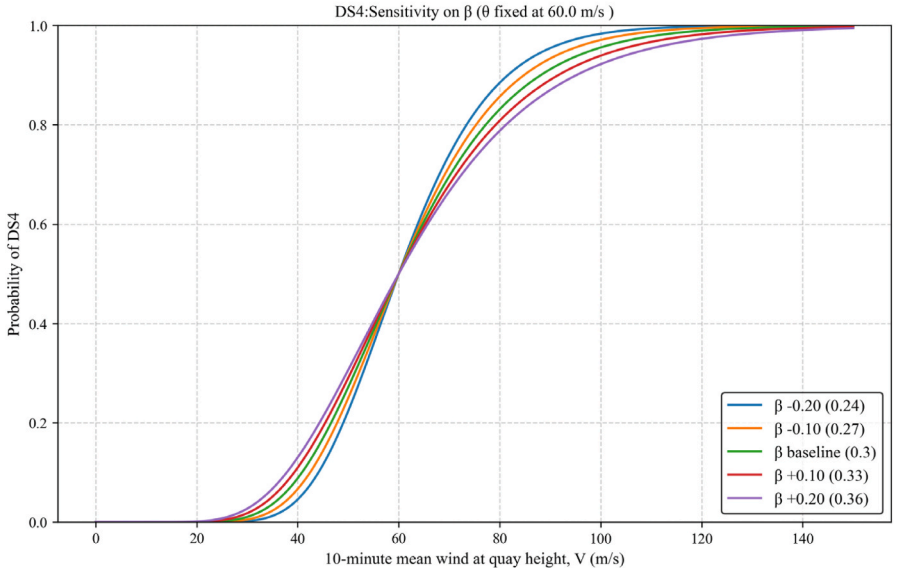

Fig. 13. (*continued*).

Table 10
Quay crane restoration curve parameters (FEMA 2024a).

Damage state	Distribution parameters		Discretized recovery probability (%)					
	Mean (days)	Std (days)	1 day	3 days	10 days	30 days	60 days	90 days
DS1	0.4	0.35	96	100	100	100	100	100
DS2	6	6	20	31	75	100	100	100
DS3	30	30	17	18	25	50	84	100
DS4	75	55	9	10	12	21	39	62

the port while allowing throughput to recover toward the intact baseline.

5.2. Economic loss estimation

The economic loss estimation across different disruption scenarios requires well-founded values for the parameters used in the

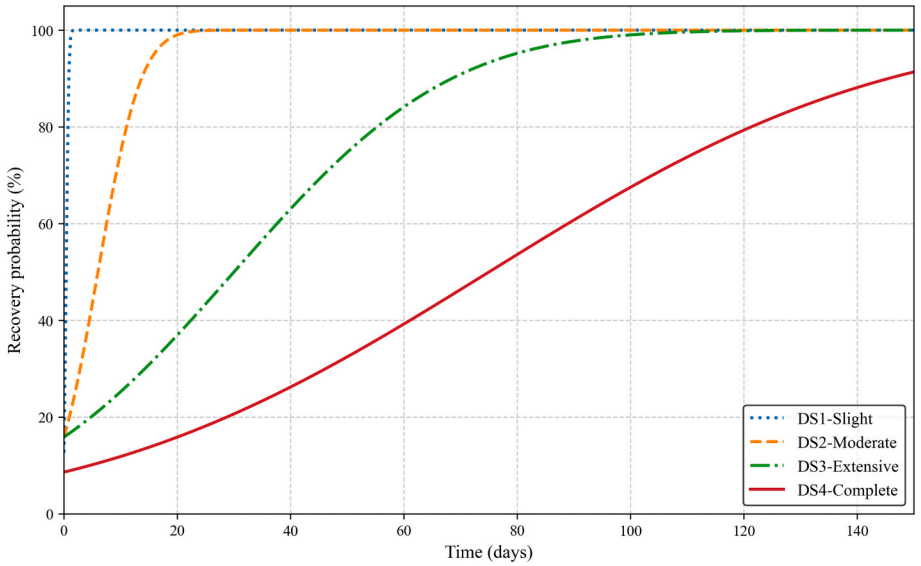

Fig. 14. The quay crane restoration curve.

Table 11
The estimated processed throughput, loss ratio, and rerouted vessels under different cyclone hazards.

Cyclone class	Output	Strike Distance Ring 1	Ring 2	Ring 3	Ring 4	Ring 5	Ring 6
TS	Processed TEU	3,635,746	3,639,253	3,643,173	3,647,709	3,647,709	3,647,709
	Loss ratio	0.33%	0.23%	0.12%	0	0	0
	Rerouted vessels	6	4	2	0	0	0
STS	Processed TEU	3,624,712	3,633,960	3,640,823	3,646,539	3,647,639	3,647,709
	Loss ratio	0.63%	0.38%	0.19%	0.03%	0	0
	Rerouted vessels	12	5	3	1	0	0
TY	Processed TEU	3,581,303	3,615,454	3,638,650	3,644,229	3,647,337	3,647,709
	Loss ratio	1.82%	0.88%	0.25%	0.10%	0	0
	Rerouted vessels	32	14	5	2	0	0
VST	Processed TEU	3,517,662	3,555,321	3,592,254	3,632,604	3,641,829	3,647,709
	Loss ratio	3.57%	2.53%	1.52%	0.41%	0.16%	0
	Rerouted vessels	68	41	25	7	3	0
VTY	Processed TEU	3,421,385	3,484,402	3,551,222	3,593,077	3,625,281	3,643,791
	Loss ratio	6.21%	4.48%	2.65%	1.50%	0.62%	0.11%
	Rerouted vessels	117	75	41	23	8	3

equations developed in Section 3.3. To this end, a comprehensive data collection effort was undertaken to obtain parameter values from the most recent and publicly available sources. These values were derived from official tariff schedules, government press releases, supplier contracts, and up-to-date market indices.

Replacement cost figures for critical path items were extracted from Evergreen Marine Corporation's Terminal 7 procurement disclosures and corroborated by international contract data. To ensure transparency and illustrate the traceability of the selected values, a few key examples are outlined as follows:

Conventional quay crane prices were obtained from recent European port procurement records, which priced operator-cab-equipped units at approximately USD 12 million. The handling tariff per TEU covers stevedoring and crane usage, paid by the shipping line to the terminal operator. The rate is USD 190 for a 20-foot container and USD 220 for a 40-foot container. On a per-TEU basis, the average estimated cost is approximately USD 200. Tables 12 and 13 summarize the sample parameter values used in the analysis.

The mean loss ratios used for quay cranes (HAZUS class PEQ2) are taken from the HAZUS default port systems economic parameters (FEMA 2024a), as represented in Table 14. The PEQ2 classification and replacement-cost framework are standard in HAZUS transportation systems module. In HAZUS, these ratios represent the expected repair cost as a fraction of replacement cost conditional on the damage state, and they are applied here to cyclone losses because they are equipment-wise and damage-state-based rather than hazard-specific once the damage state is mapped.

Fig. 16 presents the estimated economic losses from cyclone events of varying intensities impacting the five concentric ring zones. Ring zone 6 is excluded because throughput losses at that distance are negligible. These economic losses are categorized into direct damage costs, downtime costs, and recovery costs.

As it can be seen, in the case of a violent typhoon event, ring zone 1 experiences the maximum economic loss, with direct damage

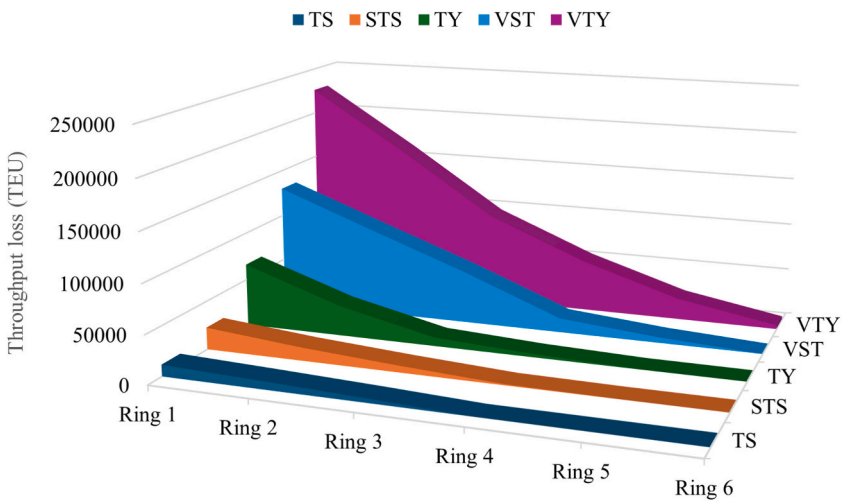

Fig. 15. The estimated throughput loss under different cyclone hazards within specified ring zones.

Table 12
The estimated asset values and relevant economic costs.

Item	Number	Price/unit ($\times 10^6$ *USD*)	Total price ($\times 10^6$ *USD*)	Representative sources
Remote-operated quay cranes	19	15	285	(Dongqi 2025)
Cabin-operated quay cranes	5	12	60	(Dongqi 2025)
Quay fenders & bollards (5 berths)	–	1	5	(CMA CGM Group, 2024; Northwest Seaport Alliance, 2025)
Shore-power sub-stations & switchgear	–	3	3	(Hitachi 2025)
5G / fibre backbone, RMS & data centre	–	15	15	(Xinhua 2022)

Table 13
Recovery and downtime cost parameter values.

Parameter	Value	Notes	Representative sources
Handling tariff	200 USD/TEU	Midpoint derived from CMA CGM Kaohsiung THC.	(CMA CGM Group, 2024)
First-increment mark-up (α)	0.15	Assumption to be calibrated with the quality/speed of recovery process.	(ElSahly et al. 2023)
Convexity exponent (β)	1.8	Assumption to be calibrated with the quality/speed of recovery process.	(ElSahly et al. 2023)
Mobilization/demobilization allowance (M)	5–7% of accelerated block costs	Extracted from USACE cost-estimating guidance & MOB/DEMOB payment practices	(Cost MCX, 2023)
Maintenance tech wages	120 USD/day	Fluctuates based on contractor method statements.	(Salary Expert, 2025)
External equipment rental	5 k-12 k USD/day	Heavy mobile crane daily rental	(BIGGE 2025)

Table 14
The mean loss ratio values for quay cranes.

Damage states	Mean loss ratio (%)	Notes
DS1	5	Minor, non-structural issues and quick fixes: sensor/calibration faults, control cabinets, drive/reeving adjustments, wheel/rail wear and re-alignment; no permanent deformation of the portal/boom.
DS2	25	Localized damage with limited steel work: bent boom tip or lashing-platform steel, trolley/reeving replacement, damaged drives/gearboxes, minor out-of-plumb corrected by jacking.
DS3	75	Major structural damage but not necessarily a total collapse: boom drop or severe distortion, portal leg buckling, sill-beam twist, machinery-house damage, crane derailment. Requires heavy-lift recovery, and large steel replacement.
DS4	100	Collapse or irreparable primary structure. Requiring demolition, debris removal, and new crane procurement.

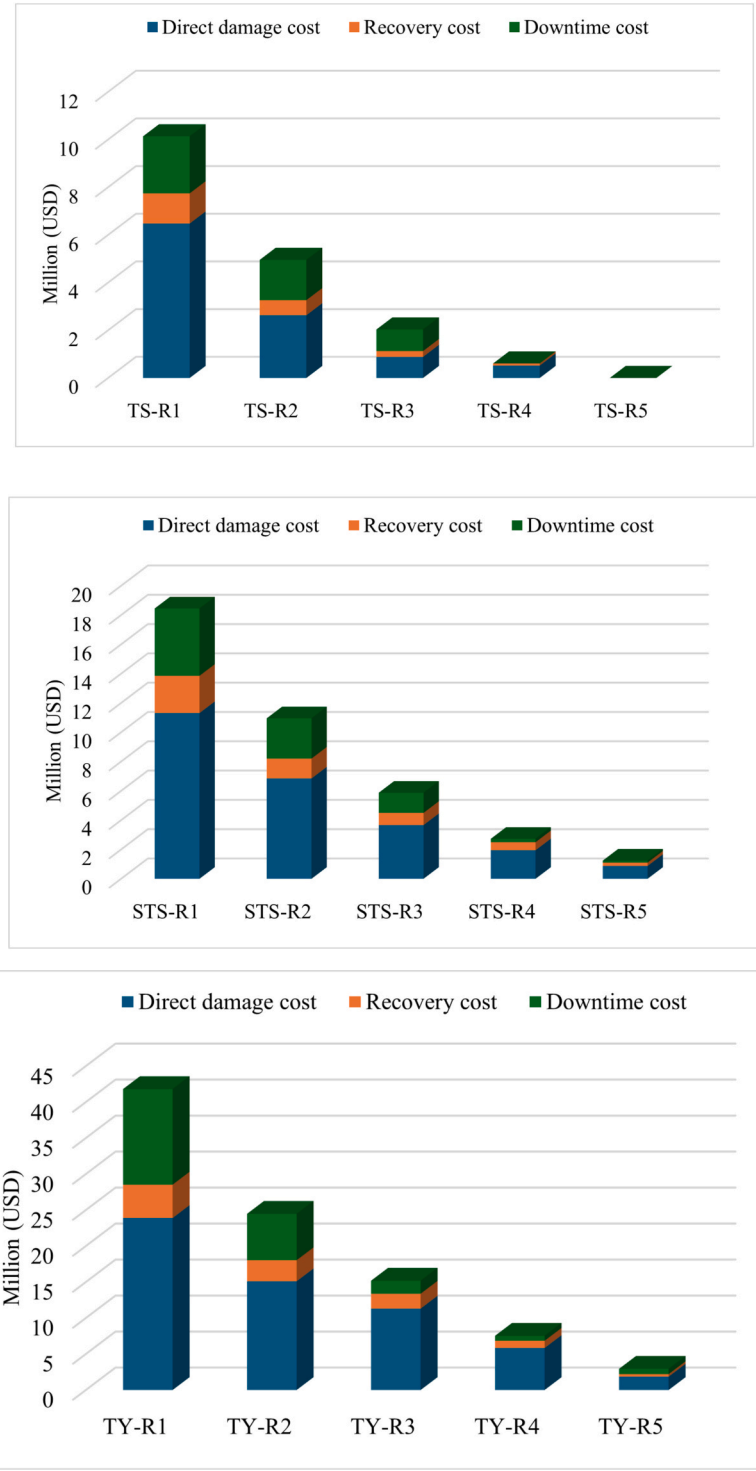

Fig. 16. The estimated economic losses due to cyclone hazards.

reaching approximately $77 million, downtime costs at around $45 million, and recovery (repair and maintenance) costs close to $16 million. Direct damage includes equipment purchases required to restore port functionalities, while the recovery cost specifically accounts for repair and maintenance activities, explicitly excluding equipment purchases. Therefore, the combined direct damage and recovery costs provide a comprehensive view of the total recovery expenses, totalling around $93 million for the most severe scenario.

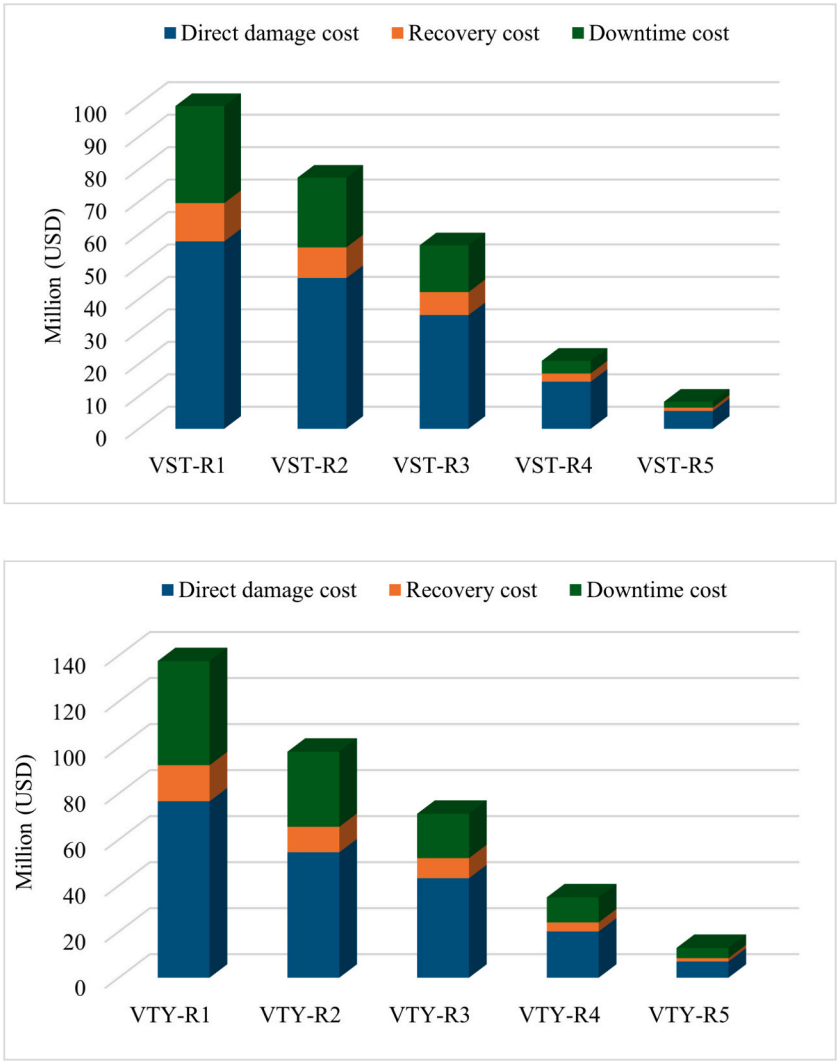

Fig. 16. (*continued*).

Fig. 16 also progressively represents less severe cyclone events, including very strong typhoon, typhoon, severe tropical storm, and tropical storm, respectively. For instance, in the case of a very strong typhoon, direct damage in ring zone 1 reduces significantly to approximately $56 million, with downtime costs decreasing to about $30 million and repair costs around $11 million. By comparison, in the case of a tropical storm, even more modest economic losses in ring zone 1 is experienced, with direct damage at approximately $6 million, downtime around $2 million, and minimal repair costs.

In these less intense events, particularly those impacting the outer ring zones, both disrupted periods and recovery durations become noticeably less significant. For example, outer rings in tropical storm scenarios exhibit direct damages below $1 million, underscoring substantially lower operational impacts compared to the innermost ring and higher intensity events.

A noteworthy aspect across all scenarios is the operational strategy implemented post-event. After the gale force period concludes and undamaged equipment is assessed, recovery processes begin concurrently with container operations using remaining intact berths and cranes. To mitigate the reduction in container throughput capacity, productivity and utilization rates of available cranes and berths are increased, compensating for the diminished operational capability due to damage.

Comparatively, these figures clearly demonstrate that economic losses significantly escalate with cyclone intensity and proximity to the central ring, with a pronounced peak for violent typhoon conditions within the innermost ring. The distinction in cost categories provides clarity on the nature of incurred expenses, highlighting the gravity of cyclones impact on the terminal operations.

5.3. *Discussion and implications*

Tropical cyclones, as previously discussed, are among the most severe natural hazards threatening the smooth operation of

seaports. Due to their destructive and catastrophic nature, they not only disrupt the immediate functionality of port operations but can also cause extensive physical damage to critical infrastructure. Quay cranes, for instance, are particularly vulnerable, and their failure may have long-lasting effects on overall port performance. Climate change has further exacerbated this challenge, with cyclone intensities projected to increase in the northwestern Pacific region, where Kaohsiung port is located. Over the next 5 years, forecasts suggest that while the frequency of storms may not necessarily rise, the region is likely to face a greater occurrence of stronger cyclones, characterized by more intense winds and heavier rainfall (Hsu and Li 2024). This serves as a warning for stakeholders and decision-makers to prepare and implement necessary actions aimed at reducing the vulnerability of port equipment through preventive and mitigative measures.

Based on the obtained results in section 5.1, from an operational perspective, tail risk is dominated by violent typhoons. In Ring 1, VTY reduces processed throughput by nearly 226 k TEU, about six percent of annual volume, and a measurable shortfall remains even at 200–400 km. In such severe events, the probability of critical damage states (DS3-DS4) rises sharply, indicating greater capacity loss, longer recovery, and thus higher throughput loss. Based on the developed fragility curves, DS3-DS4 exceedance increases steeply and nonlinearly with both intensity and proximity. As shown in Fig. 17, in Ring 1 DS4 jumps from 0.09% (TS) to 1.98% (STS), 12.01% (TY), 29.29% (VST), and 50.32% (VTY); DS3 rises in parallel as well. At Ring 2, critical damage persists for the stronger classes (VST/VTY), and by Ring 3 and 4 VTY still registers non-trivial probabilities while TS/STS are near zero. This demonstrates clear evidence of a long damage tail for high-intensity cyclones. These gradients explain why inner-ring VST/VTY dominate operational losses and diversions in our simulations.

From an economic perspective, a similar pattern emerges. In VTY Ring 1, estimated losses peak at approximately $140 million, encompassing all cost categories: direct damage, downtime, and recovery activities. VST Ring 1 reports materially lower figures, while TS Ring 1 is an order of magnitude smaller. Losses in the outer rings decline sharply for weaker storms; however, VTY and VST retain a non-trivial cost tail, reflecting persistent DS3-DS4 states and residual throughput loss. The primary driver of high direct damage costs is the DS4 class, which accounts for the majority of expected losses. A higher probability of DS4 not only increases the likelihood of direct damage but also indirectly amplifies downtime costs. This occurs for two reasons: first, the loss ratio for DS4 is set at 100%, as the damaged equipment must be fully replaced, significantly raising direct damage costs; and second, replacement times are extensive, in some cases exceeding one year, thereby prolonging downtime and associated losses.

In this regard, prioritizing resilience investments in critical-path assets, such as crane booms and drives, power systems, and the IT structures, as well as in logistics supporting both robustness and rapid field recovery is highly recommended. From a robustness perspective, such investments reduce the probability of DS3-DS4 states, where even small probability reductions can generate disproportionately large cost savings in the inner-ring zones. From a recovery perspective, modest improvements in the repair curve or spare-parts availability can significantly reduce downtime costs, thereby accelerating throughput recovery. A set of practical strategies to enhance seaport resilience to cyclones was derived from a comprehensive review of technical guidance, lessons learned from affected ports, and recent technological advances, and is summarized in Table 15.

These strategies typically require significant capital and formal risk management studies. Their merits should be assessed against (i) the local frequency and severity of cyclone hazards, (ii) the probability of relevant damage states for critical assets, and (iii) the expected throughput loss and its monetized business interruption. Using established risk frameworks and port-specific climate-resilience guidance (e.g., PIANC WG 178 and PTGCC Technical Note) helps define acceptance criteria, such as cost-benefit, risk reduction, and acceptable residual risk for adopting each option.

An instructive case is Typhoon Maemi (12 September 2003), when extreme winds in Busan triggered a domino failure of container

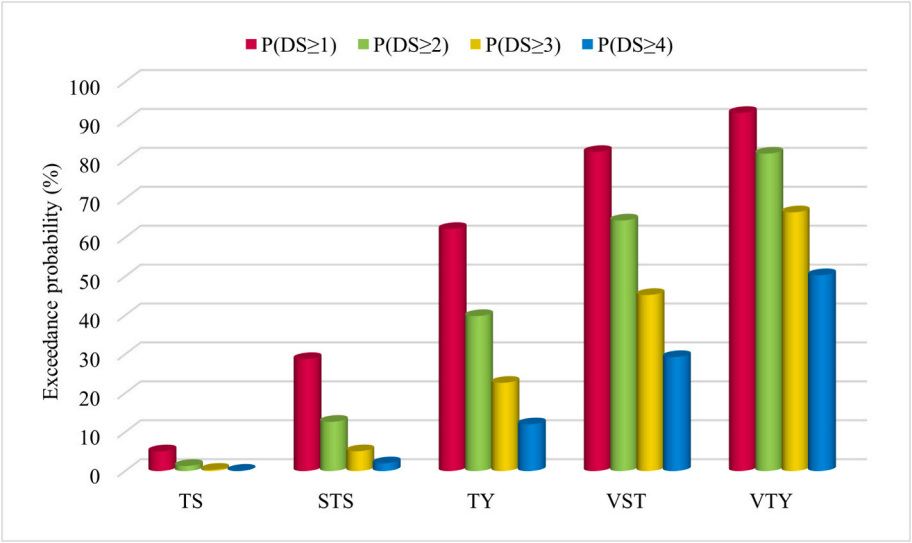

Fig. 17. The cyclone-induced damage states probabilities in Ring zone 1.

Table 15
The established resilience measure for critical path items against cyclones.

Critical path item	Measure / technology	Resilience element	Sources
Quay cranes	Ductile-link tie-downs & rail clips that prevent boom lift-off	Robustness	Typhoon Maemi post-mortem shows five-crane domino collapse would have been avoided with these links (Port Technology International)
	Boom anti-collision radar / LiDAR sensors	Robustness	Port-wide fit cuts wind-damage claims; PTI sensor trials report zero boom-ship strikes after retrofit (wpassets.porttechnology.org)
	Spare boom cradle + onsite boom ready for swap	Redundancy/Rapidity	TT-Club/ICHCA benchmark lists spare-boom strategy as best practice; swap cuts DS3-DS4 rebuild (wpassets.porttechnology.org)
	Remote diagnostics & remote crane operation centre	Rapidity/ Resourcefulness	ABB case study reports 60% of faults cleared without site visit; remote operations keep labour out of the storm zone (ABB Group)
	Mobile harbour/floating crane retained on site	Redundancy	Port New Orleans reopened three days after *Gustav* by shifting cargo to a mobile crane while STS inspections ran (FreightWaves)
Berth & mooring gear	Quick-release hooks (QRH) with integrated load pins	Robustness/Rapidity	Field data: QRH reset in minutes, limiting berth outage after surge; load-pin alarms avert line parting (Trelleborg, Interface)
	Modular composite fender panels stored on barge	Redundancy/Rapidity	Gulf terminals report swap-out in < 24 h versus 7–10 d cast-in repair (Superyacht Mooring Products)
	Floating crane for berth bypass	Redundancy/Rapidity	See New Orleans *Gustav* example (FreightWaves)
	UAV/LiDAR rapid-damage survey team on standby	Rapidity/ Resourcefulness	Post-Harvey levee survey cut inspection time by 48% over rope-access methods (LIDAR Magazine)
Power & electrical	Dual 11 kV feeder loop and auto-transfer switchgear	Redundancy/ Robustness	Specified in Bayport hurricane manual; keeps crane rails emphasize through single-circuit fault (Port Houston)
	Islandable PV + battery micro-grid for control & reefers	Redundancy/ Robustness	Port of Long Beach micro-grid designed to give 0 h outage to command centre & security hub (2022 press release) (Polb)
	Pre-staged mobile substation 115/230 kV	Redundancy/Rapidity	US-DOE study: energises blown yard transformer in 12–24 h vs 3–8 weeks full rebuild (The Department of Energy's Energy.gov)
	Hardened UPS + diesel gensets for SCADA racks	Robustness/ Redundancy	Hurricane-season UPS checklist notes 72–120 h generator autonomy for critical controls (Joe Powell and Associates, watertechonline.com)
Backbone IT / SCADA	Redundant fibre-optic ring + dual control rooms	Redundancy/ Robustness	RUGGEDCOM case: county-wide fibre ring provides path diversity and PoE for OT devices (assets.new.siemens.com)
	Hot-standby SCADA servers with automatic fail-over	Redundancy/Rapidity	VTScada guidance emphasizes N-way fail-over; no server reboot required after power dip (VTScada by Trihedral)
	Daily off-site backups & disaster-recovery	Resourcefulness/ Rapidity	IAPH Cyber-security Guidelines mandate tested backup/restore for port-wide PCS and SCADA (World Port Sustainability Program)
	SATCOM/LTE-sat hybrid for control-centre fail-over	Redundancy/ Robustness	Iridium & Hughes case studies show SATCOM terminals kept ops online when terrestrial links failed in Cat-4 storms (Iridium Satellite Communications, hughes.com)
	Secondary control centre & credentialed staff	Redundancy/ Resourcefulness	PNNL Business-continuity guideline for high-impact control centres, incl. pre-hurricane staff-up procedures (PNNL)

cranes; at the Dongbu Pusan Container Terminal, six of seven cranes collapsed sequentially, severely disrupting operations, and contemporary reports anticipated at least 15 months to fully restore the cranes (Kim et al., 2004). As a preventive measure, many ports have since specified ductile tie-down link systems for quay cranes to equalize corner uplift loads and protect quayside hardware, thereby reducing the likelihood of tie-down failure and multi-crane domino collapse under cyclone winds. Design notes and case experience also emphasize planning for spare ductile links to speed post-event recovery (UNCTAD, 2017).

Balancing investment in preventive and mitigative measures against the expected impacts of cyclone hazards, including both direct damage and downtime losses, requires a holistic, risk-informed resilience analysis, which may not be uniformly applicable across all port contexts. For large, strategically important hub ports that play critical roles in global maritime transportation networks, even short-term disruptions can propagate beyond the affected facility, triggering ripple effects and cascading failures across interconnected ports and supply chains. From a reputational perspective, prolonged disruptions may also undermine future traffic volumes and market share, as illustrated by the post-disaster recovery trajectories of Kobe Port following seismic damage and Busan Port after Typhoon Maemi, both of which experienced sustained challenges in regaining their former competitive rankings. Consequently, enhancing preparedness for disruptive events in general, and for cyclone-induced hazards in particular, necessitates that decision-makers and stakeholders systematically consider multiple technical, operational, and economic determinants within their strategic planning and investment frameworks. The proposed framework is sufficiently flexible to accommodate a wide range of resilience strategies across fully automated, semi-automated, and non-automated ports, enabling a systematic assessment of port resilience while simultaneously analysing infrastructure vulnerability and the associated economic consequences of natural-hazard-induced port disruptions.

6. Conclusions

In this paper, a risk-based simulation framework is developed and applied to Terminal 7 of the Port of Kaohsiung to assess cyclone impacts on port functionality and to estimate associated economic losses. The framework draws on operational records and detailed equipment specifications to parameterize the model and incorporates three decades of cyclone observations affecting the terminal's region to generate objective, data-driven inputs. Cyclones are first classified by type, with occurrence frequencies and intensity distributions estimated. A discrete-event simulation model in AnyLogic then quantifies functionality loss (e.g., throughput degradation

and downtime). For each scenario, direct and indirect economic impacts are evaluated using developed mathematical cost models.

The obtained results indicate the following key findings: (1) the total frequency of cyclones within 400 km of Kaohsiung Port, irrespective of type, is about 6.07 per year, with typhoon-class events accounting for 34.5%; (2) in the worst-case scenario, a violent typhoon within 50 km of the terminal, throughput loss exceeds 6% of annual volume, equating to nearly USD 45 million; (3) throughput losses diminish with lower cyclone intensity and greater distance; (4) losses are most pronounced within the first three ring zones, beyond which the impact on terminal functionality drops sharply; (5) for typhoon-class events in the near ring zones, direct physical damage costs typically exceed downtime costs; and (6) advanced resilience measures, such as boom anti-collision sensors and ductile tie-down links, can avert substantial damage and business disruption during cyclone events.

The contributions of this paper are fivefold. First, it advances current knowledge on the impacts of cyclones on port functionality and the associated economic losses. Second, it develops a dedicated cyclone hazard database for Kaohsiung Port, which can be readily extended to surrounding terminals and neighbouring ports. Third, it establishes cyclone-induced fragility curves for quay cranes, thereby improving the quantitative understanding of wind-driven damage mechanisms affecting these critical assets. Fourth, it estimates throughput loss and the resulting economic impacts using objective operational data integrated within a simulation model, thereby substantially reducing the subjectivity commonly present in comparable studies. Finally, it proposes an integrated resilience assessment framework that provides seaport authorities with a robust analytical tool to systematically evaluate, compare, and enhance resilience against climate-related hazards.

Beyond its analytical contributions, the proposed methodology offers direct practical value for port decision-makers by enabling an evidence-based assessment of the current preparedness and resilience level of individual ports, with particular relevance to cyclone-prone regions where such hazards pose an increasing threat worldwide. By jointly accounting for infrastructure vulnerability, operational performance degradation, and economic consequences, the framework functions as a holistic decision-support platform that facilitates the identification, comparison, and prioritisation of resilience strategies tailored to the specific operational context of a port. In doing so, it allows stakeholders to explicitly evaluate the trade-offs between alternative resilience investments, including their costs, benefits, and recovery implications, thereby supporting more informed, risk-based planning for sustainable and climate-resilient port infrastructure.

It is noted that the economic loss estimation in this study aims to demonstrate the applicability of the proposed methodology rather than provide precise monetary values. Publicly available and approximated data are therefore used, acknowledging that accurate estimates would require proprietary information. For port-specific applications, the cost parameters can be refined to reflect local conditions and operational realities.

Another important consideration in this study is that the characterisation of cyclone behaviour in the East Asian region is derived from an analysis of historical cyclone records over the past 30 years. While this retrospective assessment provides valuable insights into cyclone frequency and intensity, it does not fully capture a forward-looking, prognostic perspective that reflects future climatic conditions. Under climate change, both the frequency of intense events and the severity of cyclone-related hazards are expected to increase, which may alter the underlying hazard characteristics. Consequently, incorporating climate-change-informed predictive approaches is necessary to enable more realistic and robust assessments of future cyclone risks.

Future work will extend the present analysis to a multi-hazard framework that explicitly accounts for cyclone-induced effects, including storm surge, compound flooding, wave setup, run-up, and overtopping. In addition, propagating and cascading disruptions across the entire terminal system, encompassing quay, yard, and intermodal interfaces, will be systematically examined. The effectiveness of alternative resilience strategies, and their respective contributions to reducing operational disruption and associated economic losses, will also be quantitatively evaluated to support more comprehensive and actionable port resilience planning.

CRediT authorship contribution statement

Massoud Mohsendokht: Writing – review & editing, Writing – original draft, Visualization, Validation, Software, Resources, Methodology, Investigation, Formal analysis, Data curation, Conceptualization. **Ali Mokhtari-Moghadam:** Writing – review & editing, Validation, Software, Investigation, Data curation. **Huanhuan Li:** Writing – review & editing, Validation, Investigation, Formal analysis, Project administration. **Christos Kontovas:** Writing – review & editing, Validation, Supervision, Investigation. **Chia-Hsun Chang:** Writing – review & editing, Validation, Supervision, Investigation. **Zhuohua Qu:** Writing – review & editing, Validation, Supervision, Investigation. **Zaili Yang:** Writing – review & editing, Validation, Supervision, Resources, Project administration, Investigation, Funding acquisition, Formal analysis, Conceptualization.

Declaration of competing interest

The authors declare that they have no known competing financial interests or personal relationships that could have appeared to influence the work reported in this paper.

Acknowledgement

This work was supported by the European Research Council under Grant (TRUST CoG 2019 864724).

Appendix

Table A
The experts' professional profile and their related expertise.

Number	Title	Educational level	Experience	Specialization
1	General manager	MSc	20	Strategic planning, and policy implementation.
2	Operations manager	MSc	15	Cargo handling, vessel scheduling, and terminal activities.
3	Operations manager	MSc	12	Cargo handling, vessel scheduling, and terminal activities.
4	HSE director	MSc	12	Pilotage, port state control, and cargo handling
5	Professor	Ph.D.	14	Logistics and maritime transport.

Data availability

Data will be made available on request.

References

Kasm, A., Omar, A.D., Bierlaire, M., 2021. Vessel Scheduling with Pilotage and Tugging Considerations. Transportation Research Part e: Logistics and Transportation Review 148 (April), 102231. https://doi.org/10.1016/j.tre.2021.102231.

Achterkamp, J., 2019. "Improving Terminal Performance. Mega-Ships Require Mega-Terminals. Https://Www.Porttechnology.Org/".

Al-Dhaheri, N., Jebali, A., Diabat, A., 2016. The Quay Crane Scheduling Problem with Nonzero Crane Repositioning Time and Vessel Stability Constraints. Comput. Ind. Eng. 94 (April), 230–244. https://doi.org/10.1016/j.cie.2016.01.011.

Asariotis, R., Monioudi, I.N., Naray, V.M., et al., 2024. Climate Change and Seaports: Hazards, Impacts and policies and legislation for Adaptation. Anthropocene Coasts 7 (1), 14. https://doi.org/10.1007/s44218-024-00047-9.

Association, 2002. Seismic Design Guidelines for Port Structures. Taylor & Francis. https://doi.org/10.1201/NOE9026518188.

Bayazit, S., 2025. An Integrated Framework for Port-Hinterland connection Vulnerability to Sea Level rise: Izmir. Transp. Res. Part D: Transp. Environ. 142 (May), 104690. https://doi.org/10.1016/j.trd.2025.104690.

Becker, A.H., Acciaro, M., Asariotis, R., et al., 2013. A note on climate Change Adaptation for Seaports: a Challenge for Global ports, a Challenge for Global Society. Clim. Change 120 (4), 683–695. https://doi.org/10.1007/s10584-013-0843-z.

Bhimani, A., Soderberg, E., 2006. "Crane Loads & Wharf Structure Design: putting the two together. AAPA Facilities Engineering Seminar".

Bierwirth, C., Meisel, F., 2010. A Survey of Berth Allocation and Quay Crane Scheduling Problems in Container terminals. Eur. J. Oper. Res. 202 (3), 615–627. https://doi.org/10.1016/j.ejor.2009.05.031.

BIGGE. 2025. "Crane Rental Rates: What It Costs to Rent a Crane. Https://Www.Bigge.Com/Crane-Rental/Rental-Rates/?Utm_source.".

Błaszczyk, T., Nowak, M., 2009. THE TIME-COST TRADE-OFF ANALYSIS IN CONSTRUCTION PROJECT USING COMPUTER SIMULATION AND INTERACTIVE PROCEDURE. Technol. Econ. Dev. Econ. 15 (4), 523–539. https://doi.org/10.3846/1392-8619.2009.15.523-539.

Borrero, J.C., Lynett, P.J., Kalligeris, N., 2015. Tsunami Currents in ports. Philos. Trans. R. Soc. A Math. Phys. Eng. Sci. 373 (2053), 20140372. https://doi.org/10.1098/rsta.2014.0372.

Calvin, Katherine, Dipak Dasgupta, Gerhard Krinner, et al. 2023. IPCC, 2023: Climate Change 2023: Synthesis Report. Contribution of Working Groups I, II and III to the Sixth Assessment Report of the Intergovernmental Panel on Climate Change [Core Writing Team, H. Lee and J. Romero (Eds.)]. IPCC, Geneva, Switzerland. First. With Hoesung Lee. Intergovernmental Panel on Climate Change (IPCC). https://doi.org/10.59327/IPCC/AR6-9789291691647.

Camus, P., Tomás, A., Díaz-Hernández, G., Rodríguez, B., Izaguirre, C., Losada, I.J., 2019. Probabilistic Assessment of Port operation Downtimes under climate Change. Coast. Eng. 147 (May), 12–24. https://doi.org/10.1016/j.coastaleng.2019.01.007.

Cao, X., Lam, J.S.L., 2018. Simulation-based Catastrophe-Induced Port loss Estimation. Reliab. Eng. Syst. Saf. 175 (July), 1–12. https://doi.org/10.1016/j.ress.2018.02.008.

Chavas, D.R., Emanuel, K.A., 2010. A QuikSCAT Climatology of Tropical Cyclone size. Geophys. Res. Lett. 37 (18). https://doi.org/10.1029/2010gl044558.

Choi, J.S., Jin, H.H., Lee, J.J., 2022. Basic Study on the Improvement of Cargo Vehicle Parking Capacity and Parking Correction Coefficient in Port using Literature Research Method. JOURNAL of the Korean Asphalt Institute 12 (1), 90–99. https://doi.org/10.22702/JKAI.2022.12.1.8.

Christodoulou, A., Christidis, P., Bisselink, B., 2020. Forecasting the Impacts of climate Change on Inland Waterways. Transp. Res. Part D: Transp. Environ. 82 (May), 102159. https://doi.org/10.1016/j.trd.2019.10.012.

Chua, C.T., Otake, T., Li, T., et al., 2024. An Approach to Assessing Tsunami Risk to the Global Port Network under rising Sea Levels. Npj Natural Hazards 1 (1), 38. https://doi.org/10.1038/s44304-024-00039-2.

CMA CGM Group. 2024. "Taiwan Local Charges. Https://Www.Cma-Cgm.Com/Assets/Public/Documents/TAIWAN%20-%20LOCAL%20SCES%2011-06-2025_0.Pdf.".

Cost MCX. 2023. "GIWW BRAZOS RIVER FLOODGATES AND COLORADO RIVER LOCKS SYSTEMS FEASIBILITY STUDY COST ENGINEERING APPENDIX. Https://Www.Swg.Usace.Army.Mil/Portals/26/Docs/Planning/Public%20Notices-Civil%20Works/GIWW%20BRFG-CRL%20Final%20FIFR-EIS/Eng%20App%20-%20-App%2010%20-%20COST%20ESTIMATE%20%28signed%29_1.Pdf?Ver=2019-06-24-071630-927&utm_source.".

Đelović, D., 2024. Criticality Analysis of a Sea Port's Shore Cranes using Analytic Hierarchy Process Method. The Open Transportation Journal 18 (1), e26671212293095. https://doi.org/10.2174/0126671212293095240314040205.

Dongqi. 2025. "RTG vs STS Cranes: Ultimate Selection Guide. Https://Pk.Craneyt.Com/Knowledge/Rtg-vs-Sts-Cranes/.".

Dragović, B., Tzannatos, E., Park, N.K., 2017. Simulation Modelling in ports and Container terminals: Literature Overview and Analysis by Research Field, Application Area and Tool. Flex. Serv. Manuf. J. 29 (1), 4–34. https://doi.org/10.1007/s10696-016-9239-5.

Du, X., Hajjar, J.F., 2024. Methodology for Collapse Fragility Development for Hurricane events: Electrical Transmission Towers. J. Constr. Steel Res. 223 (December), 109005. https://doi.org/10.1016/j.jcsr.2024.109005.

ElSahly, O.M., Ahmed, S., Abdelfatah, A., 2023. Systematic Review of the Time-cost Optimization Models in Construction Management. Sustainability 15 (6), 5578. https://doi.org/10.3390/su15065578.

Emanuel, K., 2006. Climate and Tropical Cyclone activity: a New Model Downscaling Approach. J. Clim. 19 (19), 4797–4802. https://doi.org/10.1175/JCLI3908.1.

Emanuel, K., 2005. Increasing Destructiveness of Tropical Cyclones over the past 30 Years. Nature 436 (7051). https://doi.org/10.1038/nature03906.

Engineers, A. S. O. C. 2014. Seismic Design of Piers and Wharves. American Society of Civil Engineers. ISBN: 9780784413487.

European Committee for Standardization (CEN). 2014. "EN 13001-2: Cranes—General Design—Part 2: Load Actions. (SIST EN 13001-2:2014 Adoption).".

FEMA. 2018. “HAZUS Hurricane User Model Guide. Https://Www.Fema.Gov/.”.
FEMA. 2020. “Hazus Maritime Addendum – Hurricane Fragility Functions. Https://Www.Fema.Gov/Sites/Default/Files/Documents/Fema_hazus-Maritime-Appendix-c.Pdf.”.
FEMA. 2024a. “Hazus Earthquake Model Technical Manual Hazus 6.1.”.
FEMA. 2024b. “Hazus_6.1_Hurricane_Model_Technical_Manual. Federal Emergency Management Agency.”.
Flynn, D. 2023. “Mariner’s Tropical Cyclone Guide. Tropical Analysis and Forecast Branch; National Hurricane Center National Weather; Service National Oceanic and Atmospheric Administration.”.
Folkman, D., Gharehgozli, A., Mileski, J., Galvao, C.B., 2021. Port Resiliency and the Effects of Hurricanes on Port Operations. International Journal of Advanced Operations Management 13 (4), 4. https://doi.org/10.1504/IJAOM.2021.120779.
Geiger, T., Frieler, K., Bresch, D.N., 2018. A Global Historical Data Set of Tropical Cyclone Exposure (TCE-DAT). Earth Syst. Sci. Data 10 (1), 185–194. https://doi.org/10.5194/essd-10-185-2018.
Hamka, M.A., 2017. Safety risks assessment on container terminal using hazard identification and risk assessment and fault tree analysis methods. Proc. Eng. 194, 307–314. https://doi.org/10.1016/j.proeng.2017.08.150.
Han, D.-S., Han, G.-J., 2011. Force coefficient at each support point of a container crane according to the wind direction. Int. J. Precis. Eng. Manuf. 12 (6), 1059–1064. https://doi.org/10.1007/s12541-011-0141-5.
Hitachi. 2025. “Https://Www.Hitachienergy.Com/.”.
Hochbaum, D.S., 2016. A Polynomial Time Repeated Cuts Algorithm for the Time cost Tradeoff Problem: the Linear and Convex crashing cost Deadline Problem. Comput. Ind. Eng. 95 (May), 64–71. https://doi.org/10.1016/j.cie.2016.02.018.
Hoite, S, P McCarthy, and M Jordan. 2018. “Tie-Down Design Considerations for STS Container Cranes.” Port Technology International 77.”.
Holland, G.J., 1980. An Analytic Model of the Wind and pressure Profiles in Hurricanes. Mon. Weather Rev. 108 (8), 1212–1218.
Holton, J.R., Hakim, G.J., 2013. An Introduction to Dynamic Meteorology. Elsevier. https://doi.org/10.1016/C2009-0-63394-8.
Hossain, N.U., Ibne, F.N., Hosseini, S., Jaradat, R., Marufuzzaman, M., Puryear, S.M., 2019. A Bayesian Network based Approach for Modeling and Assessing Resilience: a Case Study of a Full Service Deep Water Port. Reliab. Eng. Syst. Saf. 189 (September), 378–396. https://doi.org/10.1016/j.ress.2019.04.037.
Hosseini, S., Barker, K., 2016. Modeling Infrastructure Resilience using Bayesian Networks: a Case Study of Inland Waterway ports. Comput. Ind. Eng. 93 (March), 252–266. https://doi.org/10.1016/j.cie.2016.01.007.
Hsu, H, and M Li. 2024. “Climate Change in Taiwan. National Scienti c Report. National Science and Technology Council and Ministry of Environment, R.O.C. (Taiwan)”.
Huang, Z., He, Z., Zhao, P., et al., 2024. The Effects of Tropical Cyclone on the Container Shipping Network: a Case Study of Typhoon Ma-on (2022). Transp. Res. Part D: Transp. Environ. 136 (November), 104449. https://doi.org/10.1016/j.trd.2024.104449.
Iai, S., 2019. Evaluation of Performance of Port Structures during Earthquakes. Soil Dyn. Earthq. Eng. 126 (November), 105192. https://doi.org/10.1016/j.soildyn.2018.04.055.
IMO. 2021. “Guidelines for Vessel Traffic Services (IMO Res. A.1158(32)). London: IMO.”.
International Taskforce, 2019. “International Taskforce Port Call Optimization, Port Call Process Handbook. Appendix to Port Call Process. Sect.
Izaguirre, C., Losada, I.J., Camus, P., Vigh, J.L., Stenek, V., 2021. Climate Change Risk to Global Port Operations. Nat. Clim. Chang. 11 (1), 14–20. https://doi.org/10.1038/s41558-020-00937-z.
Japan Meteorological Agency. 2023. “Annual Report on the Activities of the RSMC Tokyo - Typhoon Center.”.
Jian, W., Liu, C., Lam, J.S.L., 2019. Cyclone Risk Model and Assessment for East Asian Container ports. Ocean & Coastal Management 178 (August), 104796. https://doi.org/10.1016/j.ocecoaman.2019.04.023.
Kang, J.-H., Lee, S.-J., 2008. Experimental Study of Wind load on a Container Crane located in a Uniform Flow and Atmospheric Boundary Layers. Eng. Struct. 30 (7), 1913–1921. https://doi.org/10.1016/j.engstruct.2007.12.013.
Karnon, J., Stahl, J., Alan Brennan, J., Caro, J., Mar, J., Möller, J., 2012. Modeling using Discrete Event simulation: a Report of the ISPOR-SMDM Modeling Good Research Practices Task Force–4. Med. Decis. Making 32 (5), 701–711. https://doi.org/10.1177/0272989X12455462.
Jorge Rosa-Santos, P., Taveira-Pinto, F., 2013. Experimental study of solutions to reduce downtime problems in ocean facing ports: The port of Leixões, Portugal, case study. J. Appl. Water Eng. Res. 1 (1), 80–90. https://doi.org/10.1080/23249676.2013.831590.
Kim, D, B Oh, S Han, and J Shim. 2004. Collapse of Container Cranes at Busan Ports under Typhoon Maemi. In Proceedings of the Fourteenth International Offshore and Polar Engineering Conference (ISOPE).
Knaff, J.A., Sampson, C.R., DeMaria, M., Marchok, T.P., Gross, J.M., McAdie, C.J., 2007. Statistical Tropical Cyclone Wind Radii Prediction using Climatology and Persistence. Weather Forecast. 22 (4), 781–791. https://doi.org/10.1175/waf1026.1.
Konecranes. 2021. “STS Crane—Typical Technical Specification for the Fastest Ship Turnaround Time.”.
Konecranes. 2024. “Ship-to-Shore Crane (STS): Monobox Technical Document.”.
Lavelle, Francis M, Charles Goodhue, and Douglas Lyons. 2020. Critical Path Method Assessment of Community Recovery. NIST GCR 20-023. National Institute of Standards and Technology (U.S.). https://doi.org/10.6028/NIST.GCR.20-023.
Lee, S.-J., Kang, J.-H., 2008. Wind load on a Container Crane located in Atmospheric Boundary Layers. J. Wind Eng. Ind. Aerodyn. 96 (2), 193–208. https://doi.org/10.1016/j.jweia.2007.04.003.
Li, L., Wei, C., Liu, J., Chen, J., Yuan, H., 2024. Assessing Port Cluster Resilience: Integrating Hypergraph-based Modeling and Agent-based simulation. Transp. Res. Part D: Transp. Environ. 136 (November), 104459. https://doi.org/10.1016/j.trd.2024.104459.
Li, Y., Ellingwood, B.R., 2006. Hurricane damage to Residential Construction in the US: Importance of uncertainty Modeling in Risk Assessment. Eng. Struct. 28 (7), 1009–1018. https://doi.org/10.1016/j.engstruct.2005.11.005.
Liebherr Container Cranes. 2025. “Technical Description: Ship-to-Shore Gantry Cranes (STS).”.
Lu, X., Wong, W.-K., Hui, Yu., Yang, X., 2022. Tropical Cyclone size Identification over the Western North Pacific using support Vector Machine and General Regression Neural Network. Journal of the Meteorological Society of Japan. Ser. II 100 (6), 927–941. https://doi.org/10.2151/jmsj.2022-048.
Majumdar, A., Manole, I., Nalty, R., 2022. Analysis of Port Accidents and Calibration of Heinrich’s Pyramid. Transportation Research Record: Journal of the Transportation Research Board 2676 (2), 476–489. https://doi.org/10.1177/03611981211044447.
McCarthy, P, E Soderberg, and A Dix. 2009. “Wind Damage to Dockside Cranes: Recent Failures and Recommendations. TCLEE Conference.”.
Merz, B., Hall, J., Disse, M., Schumann, A., 2010. Fluvial Flood Risk Management in a Changing World. Nat. Hazards Earth Syst. Sci. 10 (3), 509–527. https://doi.org/10.5194/nhess-10-509-2010.
Miller, V., Bear-Crozier, A.N., Newey, V., Horspool, N., Weber, R., 2016. Probabilistic Volcanic Ash Hazard Analysis (PVAHA) II: Assessment of the Asia-Pacific Region using VAPAH. J. Appl. Volcanol. 5 (1), 4. https://doi.org/10.1186/s13617-016-0044-3.
Mohsendokht, Massoud, Christos Kontovas, Chia-Hsun Chang, Zhuohua Qu, Huanhuan Li, Zaili Yang. 2025. Resilience Analysis of Seaports: A Critical Review of Development and Research Directions. Maritime Policy Manage. March 23, 1–36. doi.10.1080/03088839.2025.2483410.
Mohsendokht, M., Li, H., Kontovas, C., Chang, C., Qu, Z., Yang, Z., 2026. Systemic risk analysis of complex socio-technical systems from the safety-II perspective. Reliab. Eng. Syst. Saf. 270, 112200. https://doi.org/10.1016/j.ress.2026.112200.
Na, U.J., Shinozuka, M., 2009. Simulation-based Seismic loss Estimation of Seaport Transportation System. Reliab. Eng. Syst. Saf. 94 (3), 722–731. https://doi.org/10.1016/j.ress.2008.07.005.
Northwest Seaport Alliance. 2025. “Port Fender System Replacement. Https://Www.Nwseaportalliance.Com/about-Us/Do-Business-Us/Contracting/Procurements/Pct-Fender-System-Replacement-Project-2023?Utm_source.”.
Notteboom, Theo, Athanasios Pallis, and Jean-Paul Rodrigue. 2021. Port Economics, Management and Policy. 1st ed. Routledge. https://doi.org/10.4324/9780429318184.

Pan, Q., 2015. Estimating the Economic losses of Hurricane Ike in the Greater Houston Region. Nat. Hazard. Rev. 16 (1), 05014003. https://doi.org/10.1061/(ASCE)NH.1527-6996.0000146.
Pellemans, M., Slik, J., Bhulai, S., 2025. Estimating vessel arrival times in global supply chains. Machine Learn. Appl. 22 (December), 100751. https://doi.org/10.1016/j.mlwa.2025.100751.
PEMA. 2019. "Recommended Minimum Safety Features for Quay Container Cranes. A Joint Initiative from TT Club, ICHCA International and Port Equipment Manufacturers Association. ISBN 978-1-85330-034-9.".
Pianc, 2020. "Climate Change Adaptation Planning for ports and Inland Waterways. Code: Envicom WG 178".
Port Technology International. 2024. "Evergreen Opens Kaohsiung Port's First Automated Container Terminal. Port Technology International. Https://Www.Porttechnology.Org/News/Evergreen-Opens-Kaohsiung-Ports-First-Automated-Container-Terminal/.".
Prieto, C., Patel, D., Han, D., Dewals, B., Bray, M., Molinari, D., 2024. Preface: advances in pluvial and fluvial flood forecasting and assessment and flood risk management. Nat. Hazards Earth Syst. Sci. 24 (10). https://doi.org/10.5194/nhess-24-3381-2024.
Pugh, David, and Philip Woodworth. 2014. Sea-Level Science: Understanding Tides, Surges, Tsunamis and Mean Sea-Level Changes. 1st ed. Cambridge University Press. https://doi.org/10.1017/CBO9781139235778.
Quist, P, B Wijdeven, and A.J Lansen. 2021. Part II - Ch 4 Container Terminals. Ports and Waterways: Navigating a Changing World. Editor / Mark van Koningsveld ; H.J. Verheij ; P. Taneja ; H.J. de Vriend. Delft : TU Delft OPEN Publishing, Pp. 115-160.
Rego, J.L., Li, C., 2010. Storm Surge Propagation in Galveston Bay during Hurricane Ike. J. Mar. Syst. 82 (4), 265–279. https://doi.org/10.1016/j.jmarsys.2010.06.001.
Robinson, S., 2005. Discrete-Event simulation: from the Pioneers to the present, what next? J. Oper. Res. Soc. 56 (6), 619–629. https://doi.org/10.1057/palgrave.jors.2601864.
Romano-Moreno, E., Diaz-Hernandez, G., Tomás, A., Lara, J.L., 2023. Multivariate Assessment of Port Operability and Downtime based on the Wave-Induced Response of Moored Ships at Berths. Ocean Eng. 283 (September), 115053. https://doi.org/10.1016/j.oceaneng.2023.115053.
Rosca, E., Rusca, F., Carlan, V., Stefanov, O., Dinu, O., Rusca, A., 2025. Assessing the influence of equipment reliability over the activity inside maritime container terminals through discrete-event simulation. Systems 13 (3), 213. https://doi.org/10.3390/systems13030213.
Saber, S.M., Thowai, K.Z., Rahman, M.A., Mehedi Hassan, Md., Mainul Bari, A.B.M., Raihan, A., 2025. High-Accuracy Prediction of Vessels' estimated Time of Arrival in Seaports: a Hybrid Machine Learning Approach. Marit. Transport Res. 8 (June), 100133. https://doi.org/10.1016/j.martra.2025.100133.
Salary Expert. 2025. "General Maintenance Worker. Https://Www.Salaryexpert.Com/Salary/Job/General-Maintenance-Worker/Taiwan?Utm_source.".
Sargent, R.G., 2013. Verification and Validation of simulation Models. Journal of Simulation 7 (1), 12–24. https://doi.org/10.1057/jos.2012.20.
Schott, Timothy, Chris Landsea, Gene Hafele, and Jeffrey Lorens. 2019. "The Saffir-Simpson Hurricane Wind Scale. Https://Www.Nhc.Noaa.Gov/Pdf/Sshws.Pdf. Pre20210528.".
Song, J.-J., Wang, Y., Liguang, Wu., 2010. Trend discrepancies among three best Track Data Sets of Western North Pacific Tropical Cyclones. J. Geophys. Res. Atmos. 115 (D12), 2009JD013058. https://doi.org/10.1029/2009JD013058.
Sturgis, L., Smythe, T., Tucci, A., 2014. "Port Recovery in the Aftermath of Hurricane Sandy. Center for a New American Security".
Sun, Q., Niu, X., 2021. Harbor Resonance Triggered by Atmospherically Driven Edge Waves. Ocean Eng. 224 (March), 108735. https://doi.org/10.1016/j.oceaneng.2021.108735.
TDB. 2024. "CWA RDC28 Typhoon Database Web Tool. (Https://Rdc28.Cwa.Gov.Tw/TDB/Public/Basic_query/).".
Thomas, C.M., Featherstone, W.E., 2005. Validation of Vincenty's Formulas for the Geodesic using a New Fourth-Order Extension of Kivioja's Formula. J. Surv. Eng. 131 (1), 20–26. https://doi.org/10.1061/(ASCE)0733-9453(2005)131:1(20).
Tian, Zhenshiyi, Fernando (Changyuan) Jiang, Yi Zhang, et al. 2024. "Assessing Seaport Disruption under Tropical Cyclones Using Influence Diagram and Physics-Based Modeling." Transportation Research Part D: Transport and Environment 132 (July): 104237. https://doi.org/10.1016/j.trd.2024.104237.
Toğan, V., Eirgash, M.A., 2019. Time-cost Trade-off Optimization with a New initial Population Approach. Teknik Dergi 30 (6), 9561–9580. https://doi.org/10.18400/tekderg.410934.
Touzinsky, K.F., Scully, B.M., Mitchell, K.N., Kress, M.M., 2018. Using Empirical Data to Quantify Port Resilience: Hurricane Matthew and the Southeastern Seaboard. J. Waterw. Port Coast. Ocean Eng. 144 (4), 4. https://doi.org/10.1061/(ASCE)WW.1943-5460.0000446.
Trabing, B.C., Penny, A.B., Martinez, J., Fritz, C., 2024. Are forecasts of the Tropical Cyclone Radius of Maximum Wind Skillful? Geophys. Res. Lett. 51 (12), e2024GL109663. https://doi.org/10.1029/2024GL109663.
UNCTAD. 2017. "Climate Change Impacts on Coastal Transport Infrastructure in the Caribbean: Enhancing the Adaptive Capacity of Small Island Developing States (SIDS), Climate Risk and Vulnerability Assessment Framework for Caribbean Coastal Transport Infrastructure. UNDA Project 1415O.".
UNDRR. 2019. "Global Assessment Report on Disaster Risk Reduction, Geneva, Switzerland, United Nations Office for Disaster Risk Reduction (UNDRR). eISBN: 978-92-1-004180-5.".
Usace, 2019. "EP 1100-1-5 Guide to Resilience Practices. Https://www. Publications. Usace. Army. Mil/Portals/76/EP%201100-1-5.Pdf".
Verschuur, J., Koks, E.E., Li, S., Hall, J.W., 2023. Multi-Hazard Risk to Global Port Infrastructure and Resulting Trade and Logistics losses. Commun. Earth Environ. 4 (1), 5. https://doi.org/10.1038/s43247-022-00656-7.
Wan, C., Yuan, J., Cao, D., Wang, T., Ng, A.K., 2024. A Fuzzy Evidential Reasoning-based Model for evaluating Resilience of ports to Typhoons. Transp. Res. Part D: Transp. Environ. 133 (August), 104228. https://doi.org/10.1016/j.trd.2024.104228.
Wang, N., Min, Wu., Yuen, K.F., 2023. Assessment of Port Resilience using Bayesian Network: a Study of strategies to Enhance Readiness and Response Capacities. Reliab. Eng. Syst. Saf. 237 (September), 109394. https://doi.org/10.1016/j.ress.2023.109394.
Wang, T., Zhuohua, Qu., Yang, Z., Nichol, T., Clarke, G., Ge, Y.-E., 2020. Climate Change Research on Transportation Systems: climate risks, Adaptation and Planning. Transp. Res. Part D: Transp. Environ. 88 (November), 102553. https://doi.org/10.1016/j.trd.2020.102553.
Wu, L., Jia, S., Wang, S., 2020. Pilotage Planning in Seaports. Eur. J. Oper. Res. 287 (1), 90–105. https://doi.org/10.1016/j.ejor.2020.05.009.
Wu, X., Sun, Y., Yue, Wu., Ning, Su., Peng, S., 2022. The Interference Effects of Wind load and Wind-Induced Dynamic Response of Quayside Container Cranes. Appl. Sci. 12 (21), 10969. https://doi.org/10.3390/app122110969.
Xia, W., Mishra, J., Adulyasak, Y., 2024. Seaport Adaptation and Capacity Investments under Inter-Port Competition and Climate-Change uncertainty. Transp. Res. Part D: Transp. Environ. 130 (May), 104183. https://doi.org/10.1016/j.trd.2024.104183.
Xinhua. 2022. "Europe's First 5G-Operated Logistics Terminal Opens in Hungary. Https://Www.Globaltimes.Cn/Page/202210/1277443.Shtml?Utm_source.".
Xu, M., Zhu, Y., Liu, K., Ng, A.K.Y., 2024. Assessing Resilience of Global Liner Shipping Network to Tropical Cyclones. Transp. Res. Part D: Transp. Environ. 131 (June), 104189. https://doi.org/10.1016/j.trd.2024.104189.
Xue, L., Li, Y., Yao, S., 2023. A Statistical Analysis of Tropical Cyclone-Induced Low-Level Winds near Taiwan Island. Atmos. 14 (4), 715. https://doi.org/10.3390/atmos14040715.
Yamamura, E., 2016. Natural disasters and Social Capital Formation: the Impact of the Great Hanshin-Awaji Earthquake. Pap. Reg. Sci. 95 (March). https://doi.org/10.1111/pirs.12121.
Yang, Z., Ng, A.K., Lee, P.T., et al., 2018. Risk and cost evaluation of port adaptation measures to climate change impacts. Transport. Res. Part D: Transp. Environ. 61 (June), 444–458. https://doi.org/10.1016/j.trd.2017.03.004.
Yang, Z., Lau, Y.-Y., Poo, M.-P., Yin, J., Yang, Z., 2025. Port Resilience to climate Change in the Greater Bay Area. Transp. Res. Part D: Transp. Environ. 142 (May), 104681. https://doi.org/10.1016/j.trd.2025.104681.
Yu, M., Liu, X., Ji, X., Ren, Y., Guo, W., 2024. Integrated Berth Allocation and Quay Crane Assignment and Scheduling Problem under the Influence of Various Factors. IET Collab. Intell. Manuf. 6 (4), e70001. https://doi.org/10.1049/cim2.70001.

Zhang, J., Xin, X., Liao, Z., et al., 2025. Analysis of the Ripple Effects of Disruptions on Multimodal Container terminals Operations: a System Dynamics Approach. Transport. Res. Part E: Log. Transport. Rev. 202 (October), 104264. https://doi.org/10.1016/j.tre.2025.104264.
Zhu, M., Calderon, C., Ford, A., Robson, C., and Jin, J. 2025. "Digital Twin for Resilience and Sustainability Assessment of Port Facility." Sustainable and Resilient Infrastructure, July 3, 1–34. https://doi.org/10.1080/23789689.2025.2526928.
Zong, Y., Chen, X., 1999. Typhoon Hazards in the Shanghai Area. Disasters 23 (1), 66–80. https://doi.org/10.1111/1467-7717.00105.